ACS OMEGA

http://pubs.acs.org/journal/acsodf

Article

Response of Paleogene Fine-Grained Clastic Rock Deposits in the South Qiangtang Basin to Environments and Thermal Events on the Qinghai-Tibet Plateau

Zhibo Zhang,* Huan Li,* Weiqing Zheng, Scott A. Whattam, Zhijun Zhu, Weicheng Jiang, and Difei Zhao

Cite This: *ACS Omega* 2023, 8, 26458–26478

Read Online

ACCESS | Metrics & More | Article Recommendations

ABSTRACT: The Chamdo Basin is a secondary basin in the eastern part of Tibet China and is one of the most promising of petroliferous basins for new petroleum exploration. The Qamdo Basin records a complex burial history from the Mesozoic to the Cenozoic; however, the poorly constrained sedimentology of Cenozoic strata in this basin has severely obscured the overall profile and impeded further explorations of oil and gas resources. Here, we conduct whole-rock geochemical analyses of major, trace, and rare earth elements in fine-grained clastic rocks of the Paleocene Gongjue Formation, Qamdo Basin to reveal depositional environments, provenance, and tectonic setting. Petrologically, the Gongjue Formation is dominated by red fine-grained sandy mudstones/siltstones with ripple marks. The high values of the chemical index of alteration (avg. of 78.93), chemical index of weathering (avg. of 90.10), and index of compositional variability (avg. of 2.5) suggest that the basin has undergone heavy weathering. Cross-plots of La vs Th, Th vs Sc vs Zr/10, and Th vs Co vs Zr/10 reveal a continental arc tectonic setting. Paleosalinity (Sr/Ba), paleoclimate (Sr/Cu), and redox proxies (V/Cr, U/Th, and enrichment factors of Mo and U) indicate brackish to saline and oxidizing paleowater masses during deposition of the Gongjue Formation. Provenance analyses via elements and petrology reveal that sediments in the Gongjue Formation are mainly derived from intermediate–acidic rocks of the upper crust. We conclude that the first and third members are more arid climate and heavily chemically weathered than the second member. In combination with previous studies of the structural evolution of the Qamdo Basin since the Paleogene, a model is built to describe the sedimentary environment and evolution of the Qamdo Basin during transition to the Paleocene. The first and third members, i.e., the Eg^1 and Eg^3 members of the Gongjue Formation, are dominated by an oxidizing environment of seawater-saltwater, and the climate ranges from warm and humid to arid and hot, with relatively stable environmental changes. The Eg^2 member of the Gongjue Formation is dominated by an oxidizing environment of seawater-saltwater, and the climate ranges from warm and humid to arid and hot, with more frequent environmental evolution. Our model aids in better understanding of the Paleocene climate evolution of the eastern Tibetan Plateau.

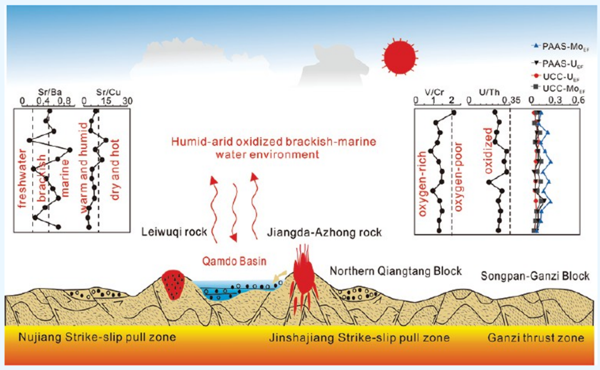

1. INTRODUCTION

The Qamdo Basin of the North Qiangtang–Qamdo block underwent three distinct evolutionary phases involving the Paleo-Tethys and Neo-Tethys and during formation within an intracontinental rifted basin.[1−5] The intracontinental rift phase forms the basic outline of the present-day configuration.[1,3,5,6] This stage is the main stage of formation of landform and mineral resources, which has attracted the attention of Chinese and overseas scholars.[7] The Chamdo Basin is a typical strike-slip pulling type basin in the northern part of the Sanjiang Tectonic Belt. $^{40}Ar/^{39}Ar$ dating,[8,9] K–Ar ages,[10] and the biostratigraphy of palynofossils and Ostracoda fossils[11] all indicate that sediments of the Qamdo Basin mainly formed in the late Eocene–early Oligocene. In sedimentological terms, since the 1990s, the sedimentary forms and tectonic framework of the filling area,[12,13] lithofacies paleogeography, and paleocurrents and sedimentary systems[14−17] have been well addressed, but there is still debate on the provenance of the Paleocene Gongjue Formation in the Qamdo Basin. Wang et al.[16] proposed that the southeastern rim of the basin was the only provenance, whereas

Received: May 7, 2023
Accepted: June 28, 2023
Published: July 12, 2023

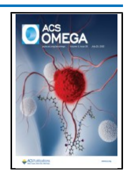

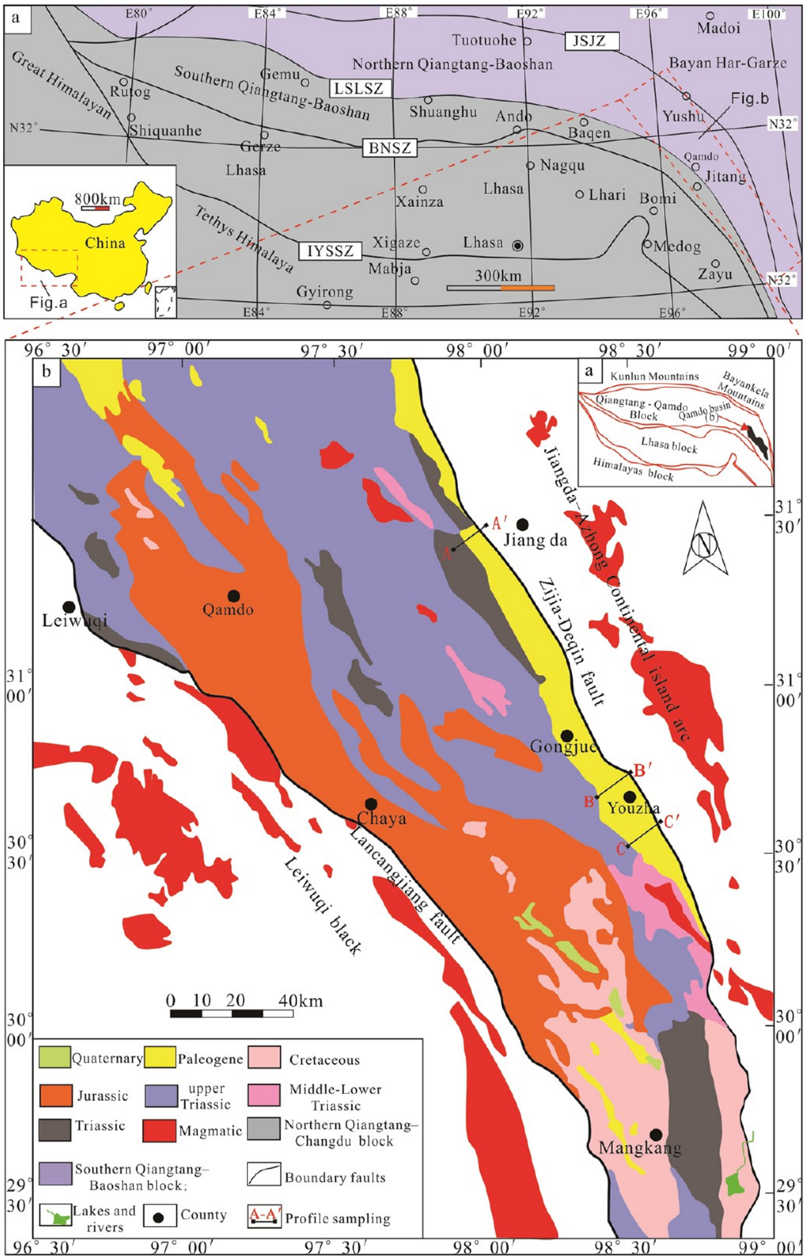

Figure 1. Regional geological map of the Qamdo Basin (modified after Fan et al.,[28] Qi,[33] and Zuo[34]).

Zhang et al.[18] believed that the provenance of this area was mainly the west in the early period and the east in the late period, based on primary sedimentary structures. In summary, the tectonic evolution, stratigraphic age, and physical origin of the Paleozoic Gongjue Formation in the Qamdo Basin have been studied, but there are two main problems. First, the source of the Paleocene Gongjue Formation is controversial, and second, the depositional environment of the Gongjue Formation has not been analyzed.

For these reasons, this paper presents a detailed analysis of the depositional characteristics, microscopic material composition, and major and trace elements of fine clastic rocks of the Paleocene Gongjue Formation. We provide evidence of the provenance, tectonic setting, and sedimentary environment of fine-grained clastic rocks of the Paleocene Gongjue Formation in the Qamdo Basin to address concerns pertaining to provenance, collision, superimposed orogenies, and paleoenvironment in the area.

2. GEOLOGICAL SETTING

2.1. Regional Geology. Located in the eastern part of the Alpine–Himalayan tectonic domain, the Tibetan Plateau has long been known as the "roof of the world". Our study area is the Qamdo Basin, located in the southeastern North Qiangtang–Qamdo block (Fig. a). The plateau has undergone a complex geological evolution, including its formation and evolution in the Paleo- to Neo-Tethyan Ocean,[19−21] which was closed along four major suture zones of the Tibetan Plateau: the Jinshajiang suture zone (JSJZ), the Longmucuo–Shuanghu–Lancangjiang suture zone (LSLSZ), the Banggong–Nujiang suture zone (BNSZ) and the Indus–Yarlung Zangbo suture zone (IYZSZ) (Figure 1a). From south to north, these sutures divide the plateau into the Tethys-Himalayan block, the Lassa–South Qiangtang–

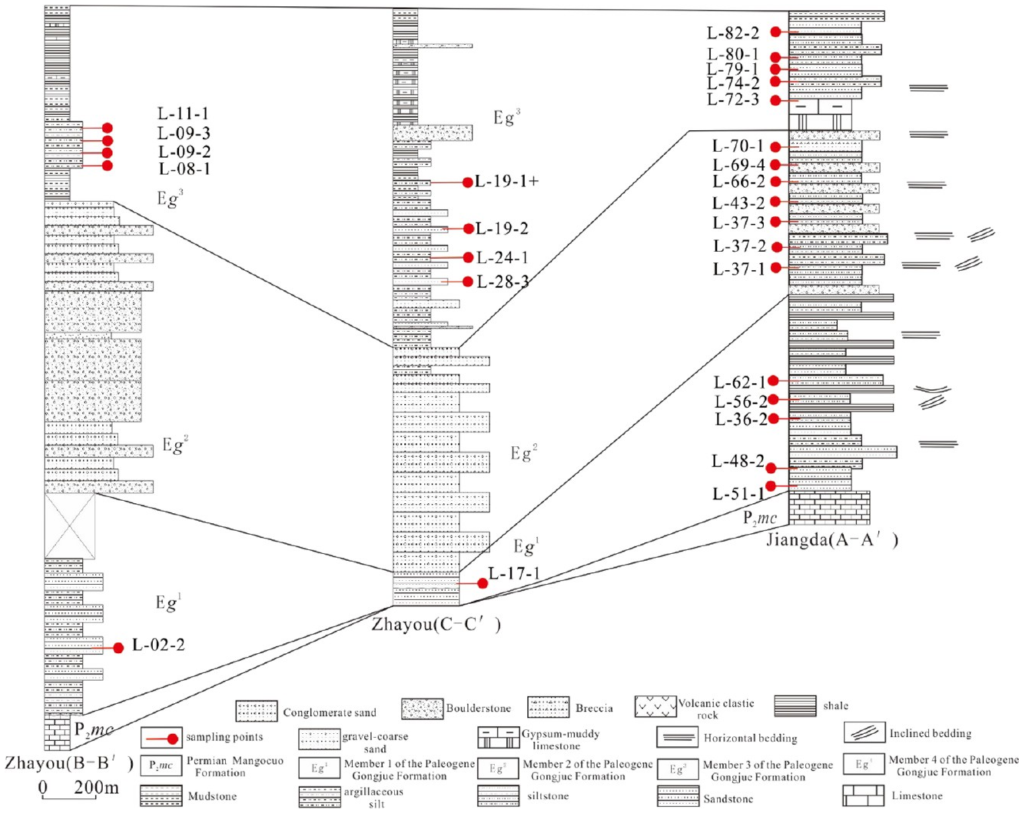

Figure 2. Summary lithologic column and sampling location of the Paleogene Gongjue Formation in the Qamdo Basin (modified after the Geological Survey Institute of Tibetan Autonomous Region[1]).

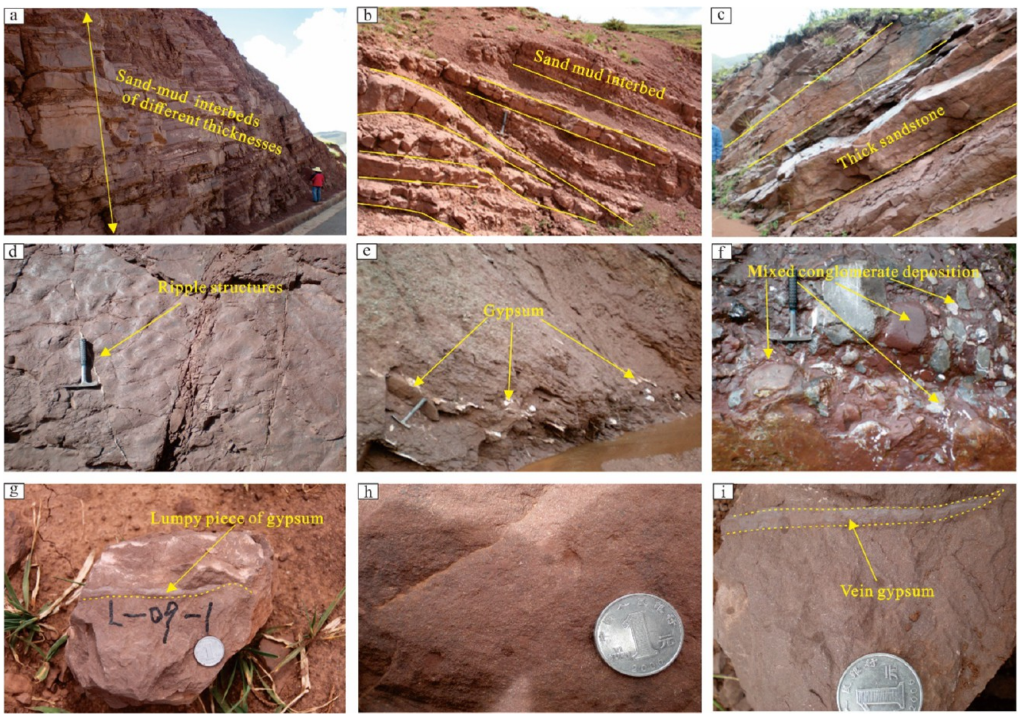

Figure 3. Field occurrences and hand specimen photos of Paleogene sedimentary rocks in the Qamdo Basin. (a) Brick red mudstone interbedded with sandstone in an unequal thickness; (b) brick red sandstone intercalated with mudstone; (c) brick red thick-layer sandstone; (d) ripple mark texture; (e) red mudstone containing gypsum; (f) mixed deposition of gypsum gravel, ash gravel, and sand gravel; (g) brick red sandstone with vein-type gypsum; (h) brick red sandstone; (i) dark red sandstone mixed with gypsum vein.

Baoshan block, the North Qiangtang−Qamdo block, and the Bayanhar−Ganzi block.[22−28] Cenozoic strata distributed mostly along the rim of the Qamdo Basin are predominantly continental and lacustrine facies and primarily composed of

https://doi.org/10.1021/acsomega.3c03144
ACS Omega 2023, 8, 26458−26478

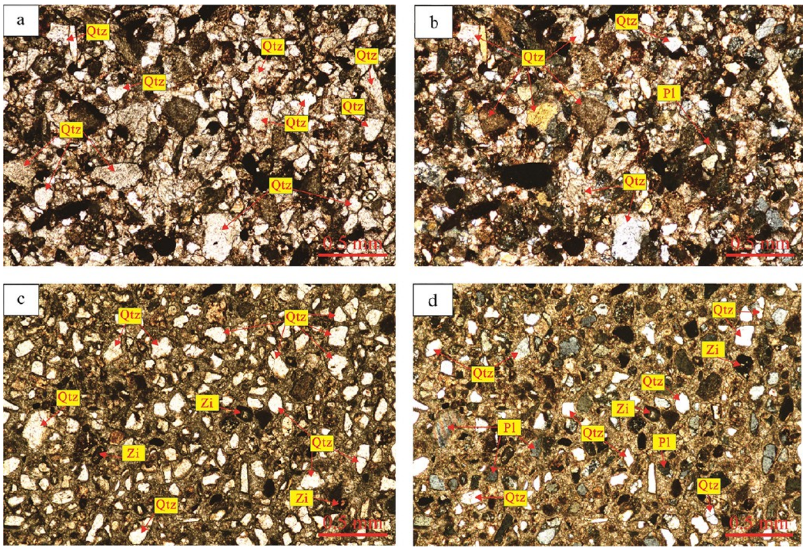

Figure 4. Microscopic observations of Paleogene clastic rocks in the Qamdo Basin. (a): Under plane-polarized light (PPL), quartz grains are cracked and fragmented with poor roundness; (b): under cross-polarized light (CPL), quartz grains are elongated with well-developed cracks; (c): under PPL, quartz grains are well sorted, and zircon and feldspar can be seen; (d): under CPL, quartz is in subangular to angular morphology and coexists with metamorphic quartz, zircon (Zi), and plagioclase feldspar.

sandstones, mudstones, and muddy limestones (Figure 1b), in addition to some fossils. Since the Paleogene, severe denudation has eroded most of the strata in the basin, except for the Gongjue Formation.[29−31] The Gongjue Formation is distributed mainly in a range of areas, such as at Leiliniang−Lelong village, Malong village in Leiwuqi County, Gongqianglong village in Qamdo County, Biezha village in Nangqian County, Long Muda village−Yuda village in Yushu County, Zedi Niuchang village, and Baima village−Suori village−Xiangpi village in Jiangda County. Rocks of the Gongjue Formation are predominantly magenta to brick-red, gray, and purple conglomerates, as well as sandstones, siltstones, and shales, which are interbedded with marlstones, limestones, gypsum rocks, sylvinites, oil shales, and copper-bearing sandstones. Some volcanic rocks, sporopollenin, Ostracoda, plants, and algae are also occasionally found in formations, with a wide range of thicknesses.[32]

2.2. Sedimentary Characteristics. Paleocene strata in the Qamdo Basin are mainly composed of continental red clastic rock deposits. Close observations and detailed descriptions of representative outcropping sections can provide insights into the recognition and interpretation of facies changes. Therefore, the A-A′, B-B′ and C-C′ sections in the Jiangda and Youzha areas were chosen to plot field lithological histograms (Figure 2). In lithological terms, the Gongjue Formation can be divided into four members.

The first lithological member of the Gongjue Formation (Eg^1) is distributed in the western part of the Qamdo Basin, and its lower part is dominated by purple−red argillaceous siltstones. Mudstones have developed in the northern rim of the Suojia member. Lithic sandstones and argillaceous siltstones are found in the southern part of the Bengbai area (Figure 3a). There are purple−red lithic sandstones intercalated with thin variegated conglomerates and siltstones, as well as local basal conglomerates. The thickness of each stratum tends to increase from south to north. The central part is mainly composed of purple−red gravel sandstones, lithic sandstones, and siltstones, with interbedded sandstones and mudstones. As observed under the microscope, the sandstones are mainly composed of angular quartz and are likely dominated by near-source deposits (Figure 4a). The upper variegated mudstones contain small amounts of argillaceous siltstones and gravel-bearing limestones. Developed lithic sandstones and argillaceous siltstones are found in the southern part of the Bengbai area.[1,4−6,35] In summary, the first member of the Gongjue Formation is a system of lacustrine facies deposits.

The second lithological member of the Gongjue Formation (Eg^2) is distributed in the eastern and western parts of the Qamdo Basin. It is distributed in unconformities in the eastern part of the basin, where it contacts Triassic strata, as well as in parallel unconformities in the basin above the first member (Eg^1). The lithology includes fine-grained sandstones, gravel-bearing coarse-grained sandstones, fine-grained gravel-bearing sandstones, lithic sandstones, and argillaceous sandstones (Figure 3b,f). Microscopic observations reveal that the coarse-grained gravel-bearing sandstones have relatively large grain sizes, indicating a dominantly near-source deposit (Figure 4b). The thickness of each stratum tends to decrease gradually from south to north.[1,4−6,35] In summary, the second member of the Gongjue Formation is transitional from riverine facies deposits in the north to Lake Facies deposits in the south.

The third lithological member of the Gongjue Formation (Eg^3) has experienced a dramatic change in the western part of the Youzha area of the Qamdo Basin and is located mainly in the compound syncline part of the Qamdo Basin. In lithological terms, it is mainly composed of gypsums, mud conglomerates, and variegated mud shales, with interbedded sands and mudstones. The bottom is dominated by conglomerates and gravel-bearing sandstones. Mixed deposits of brick-red sandy conglomerates, light gray-limestone gravels, and white gypsum gravels can be identified in the conglomerate deposits. The gypsums are vein-like (Figure 3e,f,g) and dominated by purple−red lithic sandstones and argillaceous siltstones; the central part is mainly composed of magenta lithic sandstones and argillaceous siltstones; the upper part is dominated by gypsums, argillaceous conglomerates, and variegated shales (Figure 3h,i), with wave ripple structures (Figure 3d), suggesting a shallow lacustrine environment. Microscopy shows that the variegated mud shales are mainly composed of quartz and feldspars. Mud

https://doi.org/10.1021/acsomega.3c03144
ACS Omega 2023, 8, 26458−26478

Table 1. Major Oxide (in wt % Element) Concentrations of Gongjue Formation Fine-Grained Clastic Rock Samples in the Qamdo Basin[a]

sample no	lithology (F. m)	sampling points	SiO_2	Al_2O_3	Fe_2O_3	MgO	CaO	Na_2O	K_2O	MnO	TiO_2	P_2O_5	LOI[1]	FeO	CIA	CIW	ICV
L-08-1	fine-grained sandstone (Eg^3)	Youzha (B-B′)	38.58	7.36	2.63	0.77	27.32	0.17	1.19	0.11	0.48	0.04	21.09	0.35	84.33	97.64	4.44
L-09-2	siltstone (Eg^3)	Youzha (B-B′)	56.99	10.95	4.28	2.06	10.80	1.08	1.96	0.089	0.70	0.11	10.14	0.80	78.17	90.89	1.91
L-09-3	siltstone (Eg^3)	Youzha (B-B′)	54.36	9.67	4.38	1.83	14.43	1.09	1.52	0.12	0.86	0.12	10.25	0.75	78.63	89.72	2.51
L-11-1	fine-grained sandstone (Eg^3)	Youzha (B-B′)	59.61	10.02	2.86	1.85	10.00	0.16	1.48	0.085	0.53	0.10	12.71	1.00	85.92	98.40	1.69
L-19-1[+]	fine-grained sandstone (Eg^3)	Youzha (C-C′)	73.82	6.44	2.26	0.91	7.92	1.03	0.95	0.11	0.55	0.08	5.10	0.45	76.33	86.02	2.13
L-19-2	siltstone (Eg^3)	Youzha (C-C′)	57.83	11.34	5.01	3.68	8.16	0.87	2.17	0.14	0.67	0.14	9.37	1.95	78.78	92.77	1.83
L-24-1	siltstone (Eg^3)	Youzha (C-C′)	54.96	10.40	4.48	1.60	13.82	1.79	1.44	0.09	0.81	0.11	9.46	0.65	76.14	85.11	2.31
L-28-3	fine sandstone (Eg^3)	Youzha (C-C′)	49.05	13.58	3.36	0.91	17.29	0.15	2.11	0.07	0.51	0.07	12.53	0.15	85.72	98.89	1.80
L-72-3	fine-grained sandstone (Eg^3)	Jiangda (A-A′)	55.00	8.85	3.78	1.34	15.48	1.13	1.23	0.10	0.69	0.07	11.63	1.00	78.82	88.52	2.68
L-74-2	fine-grained sandstone (Eg^3)	Jiangda (A-A′)	58.14	7.86	2.60	1.04	14.92	1.04	1.25	0.12	0.45	0.08	11.65	0.65	77.31	88.15	2.73
L-79-1	siltstone (Eg^3)	Jiangda (A-A′)	59.44	10.94	3.94	1.85	10.49	1.09	1.85	0.09	0.58	0.11	8.85	1.00	78.72	90.81	1.82
L-80-1	siltstone (Eg^3)	Jiangda (A-A′)	57.15	11.45	4.13	1.95	10.48	0.95	2.05	0.08	0.62	0.12	10.34	1.10	79.15	92.22	1.77
L-82-2	siltstone (Eg^3)	Jiangda (A-A′)	60.18	7.74	2.87	1.16	13.26	1.37	1.16	0.16	0.49	0.1	10.55	0.60	75.20	84.76	2.64
L-37-1	quartz sandstone (Eg^2)	Jiangda (A-A′)	80.52	6.86	1.97	0.65	3.19	2.88	0.44	0.07	0.32	0.08	2.60	0.80	67.08	70.10	1.39
L-37-2	fine-grained sandstone (Eg^2)	Jiangda (A-A′)	72.52	12.73	4.21	1.67	1.06	1.46	1.96	0.04	0.66	0.12	3.35	2.35	78.73	89.59	0.87
L-37-3	quartz fine sandstone (Eg^2)	Jiangda (A-A′)	72.81	8.40	3.70	1.25	4.89	2.12	0.78	0.14	0.63	0.11	4.71	1.05	74.33	79.84	1.61
L-43-2	quartz sandstone (Eg^2)	Jiangda (A-A′)	26.41	3.42	1.03	1.13	36.73	0.44	0.83	0.09	0.17	0.04	28.23	0.30	72.81	88.44	11.82
L-66-2	siltstone (Eg^2)	Jiangda (A-A′)	61.99	10.31	3.57	1.50	9.73	1.14	1.68	0.09	0.59	0.11	8.54	0.90	78.41	89.90	1.78
L-69-4	fine-grained sandstone (Eg^2)	Jiangda (A-A′)	50.66	8.60	3.77	1.56	17.84	1.05	1.41	0.15	0.71	0.11	12.98	0.90	77.64	88.96	3.08
L-70-1	siltstone (Eg^2)	Jiangda (A-A′)	56.34	9.58	3.47	1.46	13.77	1.18	1.62	0.14	0.53	0.1	10.94	1.00	77.26	88.88	2.31
L-02-2	fine-grained sandstone (Eg^1)	Youzha (B-B′)	78.58	9.89	4.59	1.12	0.49	1.31	1.26	0.02	0.44	0.14	1.89	1.15	79.32	88.23	0.93
L-17-1	pelitic siltstone (Eg^1)	Youzha (C-C′)	57.07	12.61	3.55	0.57	12.01	0.22	2.08	0.037	0.66	0.10	10.54	0.25	84.55	98.26	1.52
L-48-2	pelitic siltstone (Eg^1)	Jiangda (A-A′)	58.61	11.84	4.45	1.46	10.16	1.39	2.18	0.09	0.62	0.12	8.32	0.75	76.72	89.34	1.72
L-51-1	siltstone (Eg^1)	Jiangda (A-A′)	46.80	6.75	3.06	1.13	22.65	0.82	1.31	0.08	0.34	0.05	16.01	0.65	75.90	89.01	4.35
L-36-2	siltstone (Eg^1)	Jiangda (A-A′)	45.15	10.15	3.28	1.08	20.04	0.19	1.31	0.07	0.46	0.05	18	0.30	87.10	98.13	2.60
L-56-2	siltstone (Eg^1)	Jiangda (A-A′)	60.73	10.69	2.97	0.41	12.13	0.18	1.38	0.05	0.48	0.07	10.35	0.15	87.24	98.32	1.65
L-62-1	argillaceous fine sandstone (Eg^1)	Jiangda (A-A′)	61.41	11.63	3.91	1.25	9.36	1.01	1.74	0.12	0.67	0.12	7.98	0.35	80.78	91.89	1.55
min			80.52	13.58	5.01	2.06	36.73	2.88	2.18	0.16	0.86	0.14	28.23	2.35	87.24	95.73	0.87
max			26.41	3.42	2.26	0.41	1.06	0.15	0.44	0.02	0.32	0.04	2.60	0.15	67.08	82.27	11.82
average			57.95	9.63	3.49	1.38	12.90	1.01	1.49	0.09	0.56	0.10	10.67	0.79	78.93	90.10	2.50

[a]Note: CIA = molar $[(Al_2O_3)/(Al_2O_3 + CaO^* + Na_2O + K_2O)] \times 100$, CIW = $[Al_2O_3/(Al_2O_3 + CaO^* + Na_2O)] \times 100$, and ICV = $(Fe_2O_3 + K_2O + Na_2O + CaO + MgO + MnO + TiO_2)/Al_2O_3$.

https://doi.org/10.1021/acsomega.3c03144
ACS Omega 2023, 8, 26458−26478

Table 2. Trace Element Compositions of the Paleogene Gongjue Formation in the Qamdo Basin (ppm)

sample no	Sc	V	Cr	Co	Ni	Cs	Cu	Zn	Ga	Rb	Sr	Nb	Mo	Sb	Ba	Ta	Pb	Th	U	Zr	Hf
L-08-1	7.11	71.80	33.50	8.56	21.80	4.33	12.90	37.90	7.86	56.50	107.00	8.11	0.25	2.11	206.00	0.59	16.00	6.79	1.48	142.00	3.92
L-09-2	10.00	68.00	58.60	11.20	28.50	6.76	25.50	59.40	12.50	83.70	135.00	13.40	0.34	1.26	303.00	0.98	19.30	10.70	2.83	214.00	5.92
L-09-3	9.03	78.30	56.40	8.41	23.70	3.90	26.70	48.10	10.10	57.80	126.00	13.70	0.29	1.35	209.00	0.99	15.10	11.10	2.69	269.00	7.40
L-11-1	7.42	52.10	42.00	10.00	25.70	5.09	17.60	57.50	9.18	59.20	264.00	10.00	0.36	0.87	1914.00	0.83	13.10	8.47	1.88	152.00	4.33
L-19-1+	4.98	48.60	56.90	5.27	13.10	1.84	16.50	26.30	6.34	32.40	137.00	10.90	0.38	0.56	152.00	0.84	9.13	7.89	2.51	323.00	8.53
L-19-2	10.70	78.80	60.20	10.60	28.00	7.48	13.10	75.90	14.70	93.00	160.00	12.70	0.54	0.91	234.00	1.09	9.01	11.10	3.33	205.00	6.14
L-24-1	10.20	80.70	54.70	9.29	20.50	3.51	23.30	51.10	11.40	60.10	131.00	13.60	1.02	1.03	586.00	1.03	16.90	11.70	3.79	240.00	7.08
L-28-3	9.49	65.90	44.90	10.70	23.70	9.49	16.30	67.10	10.90	78.60	94.80	9.51	0.27	3.53	208.00	0.72	19.00	7.89	1.38	139.00	4.28
L-72-3	10.30	70.20	71.90	9.49	23.00	2.75	17.20	48.40	10.10	51.60	127.00	12.10	0.30	0.95	219.00	0.92	16.90	9.69	2.72	271.00	7.58
L-74-2	5.76	51.70	38.40	6.40	15.80	3.87	20.00	35.40	8.21	48.90	147.00	7.85	0.17	0.50	214.00	0.60	11.60	8.39	2.09	172.00	4.86
L-79-1	8.47	65.90	44.60	10.00	22.00	5.60	28.80	55.00	11.70	70.90	104.00	10.80	0.43	0.66	235.00	0.88	17.70	9.35	2.50	170.00	4.87
L-80-1	10.70	76.10	57.70	11.80	29.20	7.95	50.20	116.00	14.70	93.20	137.00	12.60	0.50	0.96	548.00	1.02	21.90	10.90	2.78	192.00	5.39
L-82-2	6.42	52.40	39.20	6.80	16.70	3.25	32.60	39.40	8.84	47.00	118.00	9.87	0.61	0.50	170.00	0.76	13.40	8.50	2.10	177.00	5.16
L-37-1	5.51	31.90	20.80	4.84	7.85	0.95	3.41	26.10	6.74	17.00	79.70	4.55	0.13	0.30	120.00	0.38	3.34	4.79	1.24	91.50	2.49
L-37-2	10.60	75.50	39.90	9.73	17.00	6.04	61.60	60.50	14.00	80.90	65.20	10.10	0.13	0.46	239.00	0.80	4.79	9.51	2.95	209.00	5.82
L-37-3	9.22	67.20	43.00	7.95	13.30	1.98	6.99	47.60	9.89	30.80	90.80	7.71	0.10	0.49	119.00	0.59	9.24	6.80	1.97	161.00	4.73
L-43-2	3.00	26.00	15.30	3.83	13.60	6.43	7.89	19.70	4.37	39.70	661.00	3.75	0.14	0.34	179.00	0.31	8.10	3.49	1.16	62.60	1.84
L-66-2	8.83	72.10	47.60	8.96	21.40	4.28	32.30	51.80	11.50	67.20	128.00	11.00	0.22	0.56	216.00	0.84	14.10	8.80	2.59	203.00	5.77
L-69-4	10.00	91.50	57.10	9.50	27.00	3.93	25.90	50.60	10.70	61.60	158.00	12.50	0.30	1.09	213.00	0.96	12.00	9.53	2.64	183.00	5.41
L-70-1	8.23	65.50	46.60	9.04	21.70	5.06	15.20	48.80	11.30	67.60	139.00	10.30	0.22	0.73	336.00	0.85	16.40	9.17	2.36	145.00	4.18
L-02-2	6.00	38.50	50.60	8.92	22.90	1.57	8.17	45.60	8.51	37.40	41.80	6.78	0.53	0.66	110.00	0.51	7.27	5.55	1.62	176.00	4.98
L-17-1	9.33	66.00	55.20	2.63	12.40	25.00	22.60	26.80	11.60	79.50	120.00	11.60	0.41	13.70	490.00	0.89	15.90	10.60	2.28	218.00	6.46
L-48-2	10.80	81.10	59.10	11.40	26.80	5.70	37.80	61.20	13.00	87.10	110.00	11.70	0.69	1.28	357.00	0.88	19.20	10.20	2.48	160.00	4.15
L-51-1	6.92	48.90	41.20	7.61	19.80	3.12	10.70	35.50	8.12	55.40	150.00	6.27	0.17	1.02	237.00	0.49	13.10	6.15	1.29	96.70	2.71
L-36-2	9.07	64.30	42.50	8.26	25.40	9.82	13.60	59.70	10.50	61.20	195.00	8.85	0.27	1.23	227.00	0.69	17.70	9.14	1.86	155.00	4.69
L-56-2	10.60	65.10	52.10	6.14	13.90	4.55	16.50	42.40	11.10	57.60	144.00	8.98	0.46	3.00	299.00	0.69	16.00	8.47	1.67	174.00	4.78
L-62-1	8.27	67.70	57.00	9.87	19.90	4.37	30.60	50.30	10.70	63.10	211.00	11.10	0.35	0.68	234.00	0.84	15.30	10.10	2.61	246.00	6.82
average	8.41	63.77	47.67	8.41	20.54	5.50	22.00	49.78	10.32	60.70	151.16	10.01	0.35	1.51	317.56	0.78	13.76	8.70	2.25	183.21	5.20
UCC (China)	10.00	70.00	44.00	12.00	21.00	3.30	17.00	63.00	18.00	95.00	300.00	13.00	0.60	0.22	640.00	0.85	18.00	9.50	1.80	170.00	4.80

https://doi.org/10.1021/acsomega.3c03144
ACS Omega 2023, 8, 26458−26478

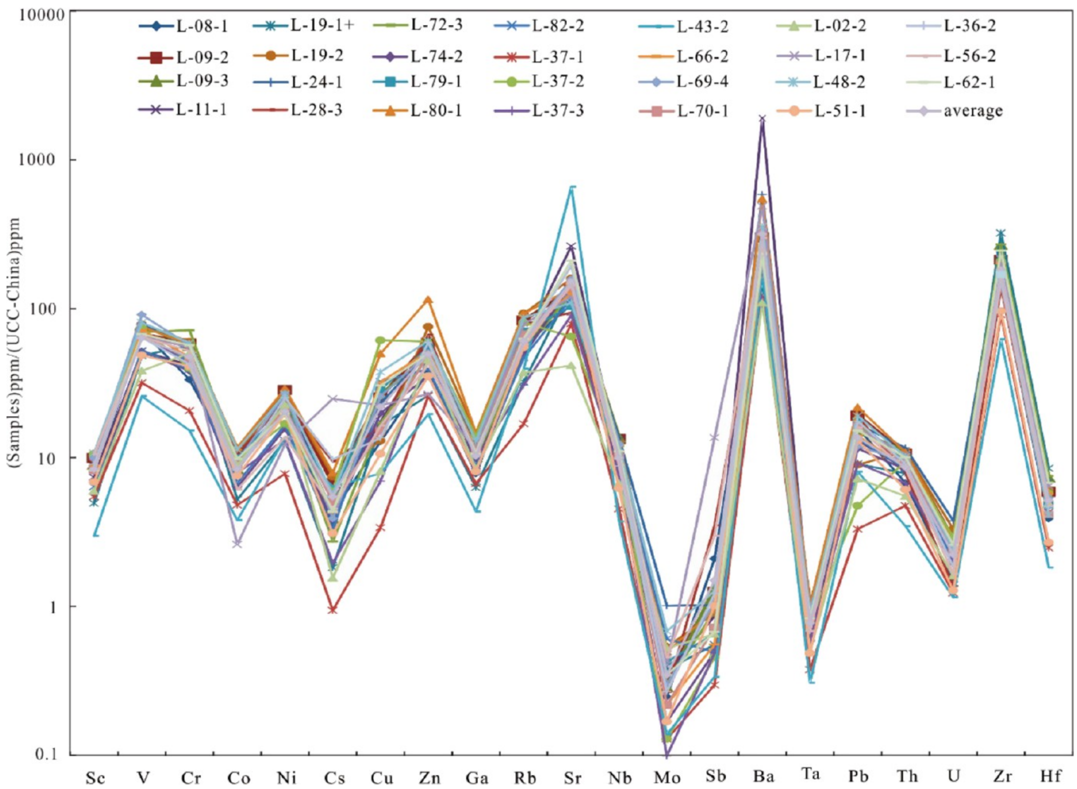

Figure 5. Trace element crust-normalized patterns (crust-normalized values are from Yan et al.[36]).

shales have small quartz grains and a small percentage of feldspars (Figure 4c,d). The thickness of the formation tends to decrease in the west and increase in the east.[1,4−6,35] In summary, the third member of the Gongjue Formation is a lake facies deposit with a hot climate.

The fourth lithological member of the Gongjue Formation (Eg^4) is distributed in the Youzha and Zongbu syncline troughs in the southern part of the Qamdo Basin. Lithologically, it is composed of siltstones, purple−red feldspar−quartz sandstones, and argillaceous siltstones that developed in the lower part and have unequal thicknesses (Figure 3c), as well as variegated shales in the central part, and coarse-grained gravel-bearing sandstones and feldspar quartz sandstones in the upper part.[1,4−6,35]

3. SAMPLING AND ANALYTICAL METHODS

Twenty-seven fresh or minimally weathered samples (fine-grained clastic rocks) of this study were collected from the first three members of the Gongjue Formation; no samples were collected from the fourth member, as it is rarely exposed and heavily weathered. The sampling sites are located in the Youzha and Jiangda areas (see the profiles named A-A′, B-B′, and C-C′ in Figure 1). Lithologically, these samples are mainly silty mudstones, siltstones, muddy limestones, and argillaceous siltstones (Figure 3).

Prior to geochemical analysis, samples were crushed to powders of 200 mesh. Major oxides were measured at the Beijing Test and Analysis Center of the Nuclear Industry by X-ray fluorescence (XRF) spectrometry. Samples (1−1.5 g) were accurately weighed before being heated in a ceramic crucible for 4 h. After being cooled for 2 h, 0.5 ± 0.05 g samples were weighed and placed in a plastic cup. $Li_2B_4O_7$ and the cosolvent were poured dropwise into the sample holder and heated for 15 min. The prepared samples were placed in a Rigaku 100e XRF for testing, with an analytical precision greater than 10%.

Trace elements were assayed by ICP−MS at the Beijing Test and Analysis Center of the Nuclear Industry. Samples were pretreated using the acid dissolution method. First, 200 mesh samples were dried at 105 °C for 3 h. Then, 50 ± 1 mg samples were weighed in a polytetrafluoroethylene dissolution container and dissolved dropwise by adding HNO_3, HF, and $HClO_4$. Finally, the Rh internal standard solution was added, and the final solution was diluted to 100.0 g with deionized water so that the concentration of Rh in the solution became 10 ng/mL. Analytical precision was greater than 5%.

The observation and microscopic thin section analysis of rocks was produced and identified at the State Key Laboratory of Nuclear Resources and Environment, East China University of Science and Technology. The polarized light projection microscope manufactured by Zeiss was based on the Axio Imager M2m model, which was used to observe and image the microscopic components and features of the rock samples.

4. RESULTS

4.1. Major Oxides. The major oxide geochemistry of the samples from the Paleocene Gongjue Formation is shown in Table 1. These Paleocene fine-grained clastic rocks have moderate to high SiO_2 contents ranging from 58.44% to 79.82% (avg. of 57.95%), Al_2O_3 of 3.42% to 13.58% (avg. of 9.63%), Fe_2O_3 of 2.26% to 5.01% (avg. of 3.49%), MgO of 0.41% to 2.06% (avg. of 1.38%), CaO of 1.06% to 36.73% (avg. of 12.90%), Na_2O of 0.15% to 2.88% (avg. of 1.01%), K_2O of 0.44% to 2.18% (avg. of 1.49%), MnO c of 0.02% to 0.16% (avg. of 0.09%), TiO_2 of 0.32% to 0.86% (avg. of 0.56%), P_2O_5 of 0.039% to 0.14% (avg. of 0.10%), loss on ignition contents of 2.6% to 28.23% (avg. of 10.67%), and FeO contents of 0.15% to

https://doi.org/10.1021/acsomega.3c03144
ACS Omega 2023, 8, 26458−26478

Table 3. REE Compositions of the Paleogene Gongjue Formation in the Qamdo Basin[a]

	m(w)ppm																					
sample no	La	Ce	Pr	Nd	Sm	Eu	Gd	Tb	Dy	Ho	Er	Tm	Yb	Lu	Y	ΣREE	LREE	HREE	LREE/HREE	La_N/Yb_N	δEu	δCe	La/Yb
L-08-1	20.10	38.10	4.46	17.40	3.21	0.79	2.94	0.55	2.94	0.58	1.73	0.28	1.70	0.25	16.90	119.03	84.06	34.97	2.40	7.97	0.77	0.93	11.82
L-09-2	30.00	59.00	7.41	28.50	5.65	1.22	4.97	0.89	4.95	0.94	2.81	0.40	2.87	0.44	26.20	186.26	131.78	54.48	2.42	7.05	0.69	0.93	10.45
L-09-3	33.70	63.40	7.84	30.00	5.68	1.20	5.04	0.85	4.64	0.85	2.53	0.41	2.53	0.42	23.90	192.01	141.82	50.19	2.83	8.98	0.67	0.91	13.32
L-11-1	24.10	49.20	5.94	23.50	4.60	1.18	4.28	0.74	4.12	0.78	2.30	0.36	2.11	0.33	23.00	153.95	108.52	45.43	2.39	7.70	0.80	0.96	11.42
L-19-1+	31.00	55.00	6.68	24.00	4.34	0.91	3.83	0.64	3.53	0.65	1.92	0.34	2.04	0.29	19.20	159.36	121.93	37.43	3.26	10.25	0.67	0.88	15.20
L-19-2	31.40	61.10	7.15	28.00	5.44	1.16	4.78	0.88	4.89	0.91	2.80	0.44	2.90	0.42	26.40	189.36	134.25	55.11	2.44	7.30	0.68	0.95	10.83
L-24-1	32.60	58.50	7.18	27.90	5.57	1.17	4.96	0.86	4.88	0.90	2.70	0.41	2.56	0.41	25.00	185.80	132.92	52.88	2.51	8.59	0.67	0.88	12.73
L-28-3	23.60	42.80	5.51	22.20	4.56	1.02	3.64	0.67	3.66	0.68	1.94	0.29	2.02	0.29	20.00	142.38	99.69	42.69	2.34	7.88	0.74	0.87	11.68
L-72-3	35.80	66.50	8.30	31.40	5.96	1.27	4.96	0.89	4.95	0.88	2.67	0.43	2.64	0.40	25.40	202.74	149.23	53.51	2.79	9.14	0.70	0.90	13.56
L-74-2	27.50	53.10	6.34	24.20	4.46	0.91	4.06	0.68	3.68	0.66	1.88	0.31	1.75	0.29	20.10	155.68	116.51	39.18	2.97	10.59	0.64	0.93	15.71
L-79-1	27.50	51.50	6.03	23.60	4.86	0.93	3.84	0.74	3.89	0.75	2.12	0.34	2.21	0.33	21.00	158.12	114.42	43.69	2.62	8.39	0.64	0.92	12.44
L-80-1	30.00	56.20	6.86	26.50	5.31	1.13	4.64	0.84	4.66	0.88	2.62	0.42	2.61	0.41	24.90	178.68	126.00	52.68	2.39	7.75	0.68	0.91	11.49
L-82-2	25.50	48.60	5.57	22.20	4.39	0.90	3.91	0.68	3.54	0.68	1.98	0.31	1.99	0.32	19.20	146.18	107.16	39.03	2.75	8.64	0.65	0.94	12.81
L-37-1	15.60	29.60	3.48	14.30	2.96	0.65	2.64	0.48	2.43	0.47	1.33	0.20	1.40	0.21	13.70	94.96	66.59	28.37	2.35	7.51	0.70	0.93	11.14
L-37-2	23.00	43.70	5.14	20.40	3.85	0.81	3.54	0.65	3.96	0.79	2.39	0.40	2.79	0.43	23.00	145.86	97.30	48.56	2.00	5.65	0.66	0.92	8.39
L-37-3	20.30	37.50	4.69	18.50	3.87	0.78	3.71	0.74	3.90	0.74	2.05	0.33	2.31	0.35	21.30	130.29	85.64	44.65	1.92	5.92	0.62	0.89	8.79
L-43-2	11.10	20.50	2.40	9.04	1.74	0.34	1.29	0.24	1.25	0.25	0.72	0.13	0.76	0.12	7.18	60.06	45.12	14.94	3.02	9.80	0.66	0.91	14.53
L-66-2	25.10	47.90	5.98	23.00	4.50	1.00	4.03	0.77	4.16	0.72	2.19	0.37	2.17	0.36	22.70	153.77	107.48	46.29	2.32	7.80	0.70	0.91	11.57
L-69-4	30.50	56.30	6.96	27.70	5.29	1.12	4.69	0.83	4.41	0.81	2.29	0.37	2.27	0.37	23.50	177.41	127.87	49.54	2.58	9.06	0.67	0.90	13.44
L-70-1	27.20	51.50	6.01	23.50	4.75	0.97	4.07	0.66	3.62	0.72	2.07	0.31	1.95	0.31	19.70	155.57	113.93	41.63	2.74	9.40	0.66	0.93	13.95
L-02-2	16.90	31.60	3.79	14.40	2.72	0.62	2.61	0.46	2.46	0.49	1.49	0.24	1.48	0.25	14.00	99.50	70.03	29.47	2.38	7.70	0.70	0.91	11.42
L-17-1	30.20	56.10	6.91	26.20	5.34	1.10	4.57	0.84	4.56	0.90	2.60	0.41	2.67	0.43	24.30	176.46	125.85	50.61	2.49	7.63	0.66	0.90	11.31
L-48-2	30.20	57.10	7.02	27.30	5.12	1.17	4.54	0.81	4.25	0.82	2.39	0.38	2.25	0.35	21.90	176.40	127.91	48.49	2.64	9.05	0.73	0.91	13.42
L-51-1	18.50	33.70	4.14	16.30	3.29	0.75	2.96	0.52	2.84	0.53	1.41	0.24	1.48	0.24	15.30	109.13	76.68	32.44	2.36	8.43	0.72	0.89	12.50
L-36-2	28.60	50.20	6.29	24.00	4.78	1.01	4.17	0.73	4.14	0.78	2.26	0.37	2.33	0.36	22.10	161.19	114.88	46.31	2.48	8.28	0.68	0.86	12.27
L-56-2	28.00	46.40	6.00	22.80	4.10	1.00	3.72	0.70	3.73	0.70	2.07	0.33	2.04	0.36	19.90	152.45	108.30	44.15	2.45	9.25	0.77	0.82	13.73
L-62-1	30.60	57.90	7.06	27.40	5.05	1.04	4.29	0.78	4.13	0.83	2.36	0.40	2.41	0.38	22.70	175.60	129.05	46.55	2.77	8.56	0.67	0.92	12.70
average	26.24	49.00	5.97	23.12	4.50	0.97	3.95	0.71	3.86	0.73	2.13	0.34	2.16	0.34	20.83	153.27	109.81	43.45	2.54	8.31	0.69	0.91	12.32
UCC (China)	33.00	64.00	7.3	28.00	5.00	1.12	4.40	0.67	4.00	0.67	4.00	0.80	2.30	0.33	18.00	155.59	138.42	17.17	8.06	9.67	0.71	0.95	9.67

[a]Note: ΣREE: rare earth element; LREE: light rare earth element; HREE: heavy rare earth element.

https://doi.org/10.1021/acsomega.3c03144
ACS Omega 2023, 8, 26458−26478

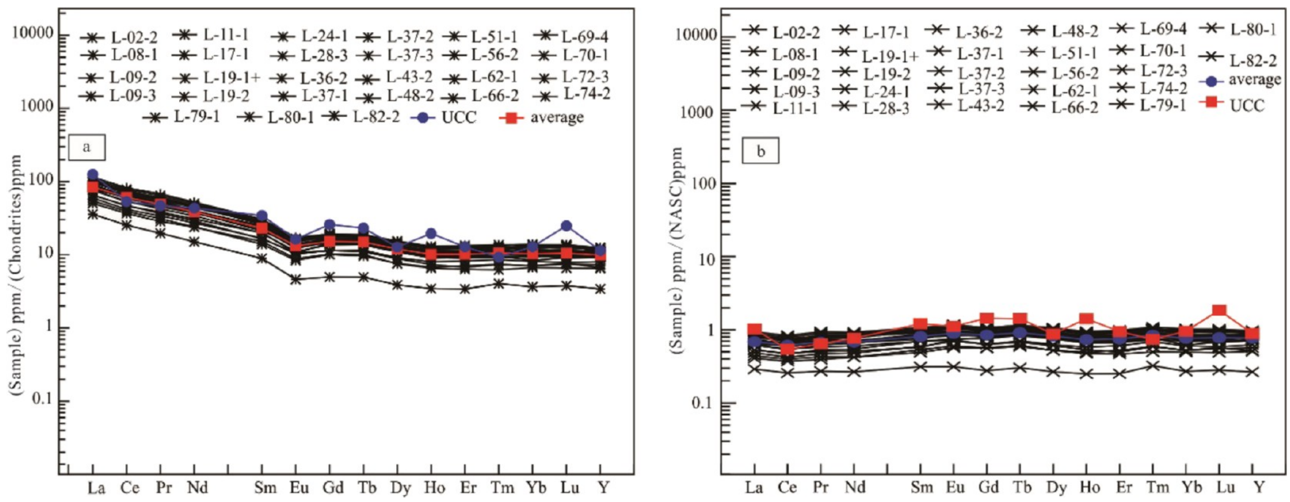

Figure 6. REE chondrite-normalized patterns and North American Shale Composition (NASC)-normalized curve of fine-grained clastic rocks of the Paleogene Gongjue Formation in the Qamdo Basin. (a) Chondrite-normalized curve of rare earth elements (Sun and McDonough[37]). (b) Normalized curve of rare earth elements in NASC (Haskin and Paster[38]).

Table 4. Comparison between Paleogene Gongjue Fine-Grained Clastic Rocks and Rocks in Different Tectonic Settings in the Qamdo Basin (ppm)

parameter	research area	Oceanic Island Arc (OIA)	Continental Island Arc (CIA)	Active Continental Margin (ACM)	Passive Margin (PM)
ΣREE	153.27	58.00 ± 10	146.00 ± 20	186.00	210.00
La/Yb	12.17	4.20 ± 1.5	11.00 ± 3.6	12.50	15.90
$(La/Yb)_N$	8.21	2.80 ± 0.9	7.50 ± 2.5	9.10	8.50
δEu	0.69	1.04 ± 0.11	0.79 ± 0.13	0.60	0.56
U	2.25	1.09 ± 0.21	2.53 ± 0.24	3.90 ± 0.5	3.20 ± 0.8
Zr	183.21	96.00 ± 20	229.00 ± 27	179.00 ± 33	298 ± 80
Nb	10.01	2.00 ± 0.4	8.50 ± 0.8	10.70 ± 1.4	7.90 ± 1.9
Y	21.20	19.50 ± 5.6	24.20 ± 2.2	24.90 ± 3.6	27.30 ± 5.3
Nd	23.55	11.36 ± 2.9	20.80 ± 1.6	25.40 ± 3.4	29.00 ± 5.03
V	63.77	131.00 ± 40	89.00 ± 13.7	48.00 ± 5.9	31.00 ± 9.9
Cr	47.67	37.00 ± 13	51.00 ± 6.5	26.00 ± 4.9	39.00 ± 8.5
Rb/Sr	0.40	0.05 ± 0.05	0.63 ± 0.33	0.89 ± 0.24	1.19 ± 0.4
Ba/Rb	5.23	21.30 ± 5.0	7.50 ± 1.3	4.50 ± 0.8	4.70 ± 1.1
Ba/Sr	2.10	0.95 ± 0.6	3.55 ± 1.4	3.80 ± 0.7	4.70 ± 1.3
Th/U	3.87	2.10 ± 0.78	4.60 ± 0.45	4.80 ± 0.38	5.60 ± 0.67
Zr/Th	21.06	48.0 ± 13.4	21.50 ± 2.4	9.50 ± 0.7	19.10 ± 5.8
Zr/Y	8.64	5.67 ± 1.94	9.60 ± 0.8	7.20 ± 0.4	12.40 ± 4.0
Nb/Y	0.47	0.11 ± 0.03	0.36 ± 0.04	0.43 ± 0.04	0.30 ± 0.06
data source	this paper	Bhatia;[44] Bhatia and Crook[45]			

2.35% (avg. of 0.79%). SiO_2 contents indicate the source of fine-grained clastic rocks; however, SiO_2 is highest and varies widely in fine-grained clastic rocks in the Qamdo Basin, while the Fe_2O_3 and MgO contents are relatively low and vary within a narrow range. The indices of chemical weathering, the chemical index of alteration (CIA), chemical index of weathering (CIW), and index of compositional variability (ICV), range from 67.8 to 87.24 (avg. of 78.93), 82.27 to 95.73 (avg. of 90.10), and 0.87 to 11.82 (avg. of 2.50), respectively.

4.2. Trace Elements. Trace element concentrations are listed in Table 2. The average contents of large ion lithophile elements (LILE), such as Cs, Rb, Sr, and Ba, are 5.50, 60.70, 151.16, and 317.56 ppm, respectively. Relatively enriched in Sr, Ba, and Zr but deficient in Cs, Mo, and Ta. Average contents of high field strength elements (HFSE), such as Sc, Nb, Ta, Zr, Hf, and Th, are 8.41, 10.01, 0.78, 183.20, 5.20, and 8.70 ppm, respectively. Among them, Ta, Mo, and U are weakly depleted. The normalized curve of crustal elements was adopted from Yan et al.[36] in Figure 5, and patterns of the curve are almost identical among all samples and close to crustal element values.

4.3. Rare Earth Elements. Total contents of REEs (ΣREE) range from 60.06 to 202.74 ppm (avg. of 153.27 ppm). Specifically, light REE (LREE) contents range from 45.12 and 149.23 ppm (avg. of 109.81 ppm), whereas heavy REE (HREE) contents range from 14.94 to 61.80 ppm (avg. of 43.45 ppm). Chondrite-normalized La/Yb (La_N/Yb_N) ratios range between 5.65 and 10.59 (avg. of 8.21), Eu/Eu* ratios (where Eu is chondrite-normalized and $Eu^* = \sqrt{[SmN \times GdN]}$) range from 0.62−0.80 (avg. of 0.69), and Ce/Ce* ratios (where Ce is chondrite-normalized and $Ce^* = \sqrt{LaN \times PrN}$) range from 0.82−0.96 (avg. of 0.91) (Table 3). Comparison between chondrite-normalized REE patterns shows that the sedimentary rocks in the Gongjue Formation are strongly enriched in LREEs but depleted in HREEs, with obvious negative Eu anomalies

https://doi.org/10.1021/acsomega.3c03144
ACS Omega 2023, 8, 26458−26478

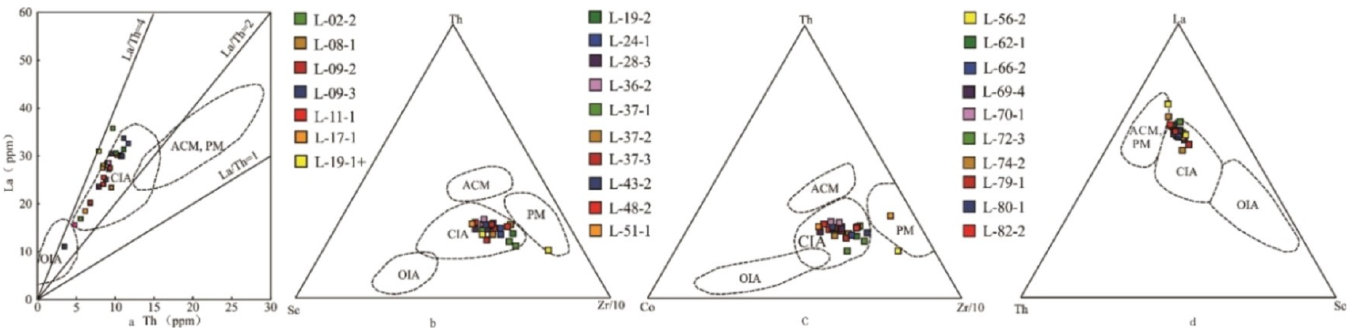

Figure 7. Diagrams for distinguishing the tectonic setting of Paleogene Gongjue sedimentary rocks in the Qamdo Basin (Bhatia and Crook[45]). (a) La vs Th. (b) Th vs Sc vs Zr/10. (c) Th vs Co vs Zr/10. (d) La vs Th vs Sc. ACM, Active Continental Margin; PM, Passive Margin; OIA, Oceanic Island Arc; CIA, Continental Island Arc.

(Figure 6a). Patterns are similar to those of North American Shale Composition (NASC) (Figure 6b).

5. DISCUSSION

5.1. Tectonic Setting. The rare earth element contents in fine-grained clastic rocks are dependent on the nature of the source area and are rarely subject to change due to tectonic activity and diagenesis. Therefore, they can provide information about the original sediments and tectonic environment in the source area.[39−43] Table 4 shows a geochemical comparison between fine-grained clastic rocks of the Paleocene Gongjue Formation in the Qamdo Basin and sandstones formed in different tectonic settings. The ΣREE, Eu/Eu*, U, Cr, Rb/Sr, Th/U, Zr/Th, and Zr/Y values of fine-grained clastic rocks of the Gongjue Formation are close to their counterparts indicative of a continental arc environment (Table 4). Zr, Nb, Y, Nd, V, Ba/Rb, and Nb/Y values in Gongjue and Qamdo rocks are also similar to their counterparts and again suggestive of formation in a continental arc setting. These data strongly suggest that the provenance of fine-grained clastic rocks of the Gongjue Formation in the study area was a continental arc environment.

Bhatia[44] studied the trace element geochemistry of ancient mudstones and graywackes under the tectonic settings of five known source areas in eastern Australia and found a correspondence of trace element contents to source types and tectonic settings. Discriminant La−Th, Th−Sc−Zr/10, Th−Co−Zr/10, and La−Th−Sc diagrams were proposed for sedimentary rocks that formed in different tectonic environments. These diagrams were confirmed as an effective and intuitive approach to reveal the tectonic environment of graywackes.[35] The geochemistry of fine-grained clastic rocks can be inherited from the source area.[24,26] Therefore, the tectonic environment of fine-grained clastic rocks of the Paleocene Gongjue Formation in the Qamdo Basin was identified using the ternary diagram of La−Th, Th−Sc−Zr/10, Th−Co−Zr/10, and La−Th−Sc (Figure 7). Most samples plot within the continental arc environment, apart from a small minority that plot within a passive continental rim environment.

In summary, analysis of the provenance of the Paleocene Gongjue Formation in the Qamdo Basin in conjunction with results from previous research shows that Paleocene materials in the Qamdo Basin were sourced mostly from a continental arc environment.

5.2. Paleoclimate Reconstruction. Sr content depends on CaO content, and Cu content is related to organic carbons and paleoproductivity.[46,47] The Sr and CaO contents in the study area are weakly interrelated; additionally, the study area is dominated by red fine-grained rocks, with extremely rare organic carbons and hence extremely low paleoproductivity. Thus, influences of the CaO content, organic carbon, and paleoproductivity on Sr and Cu contents can be eliminated.[48] The Sr/Cu ratio is often used to show paleotemperature and humidity. The Sr/Cu ratio indicates a warm and humid climate if it ranges between 1 and 10 but signifies a dry and hot climate if >10.[20,49,50] The Sr/Cu ratios of fine-grained clastic rocks in the first and third members of the Gongjue Formation vary slightly between 2.91 and 14.34 and between 2.73 and 15.00, respectively (Table 4). The Sr/Cu ratios of the counterparts in the second member (Eg^2) range from 1.06 to 83.78, which are in sharp contrast to those in the other two members (Eg^1 and Eg^3). Overall, the variation in the Sr/Cu ratios among all the samples from these three members is indicative of the complex paleoclimate under which the Gongjue Formation formed; that is, the climate might have changed continuously from warm to hot and from humid to dry, and vice versa (Figures 11 and 12b).

5.3. Provenance Analysis. The geochemistry of clays and silty rocks can best indicate the material composition of sedimentary provenance.[40,50,51] Generally, immobile trace elements (e.g., Sc, Nb, Hf, Th, Zr, Y, etc.) are capable of maintaining their original concentrations throughout sedimentary processes, such as weathering, denudation, and transport, which is conducive to determining the geochemistry of source rocks.[51−55] Moreover, rare earth elements (REEs) are considered relatively immobile, and their contents in sediments are less subject to post-modification, including weathering and erosion. Consequently, REE distribution patterns are likely to remain unchanged during sedimentation and diagenesis[56] and thus can be employed to unmask provenance signatures. In contrast, initial contents of mobile Ca, Na, and K oxides that have undergone a series of post-modification, such as weathering, denudation, transport, sedimentation, and diagenesis, are highly mobile.[39,57,58] Therefore, major element oxides are widely used to estimate the weathering−alteration degree of sedimentary rocks.[59,60] Due to K metasomatism and cyclic sedimentation, the chemical index of alteration (CIA) of the chemical weathering process, which affects the reliability of its products, can be overestimated. Therefore, the index of compositional variability (ICV) is used for correction. If ICV > 1, the fine-grained clastic rocks contain little clay material, indicating initial deposition in an active tectonic belt; if ICV < 1, the fine-grained clastic rocks contain much clay material, that is, the sediments have experienced sedimentary recycling or initial deposition under heavy weathering.[59,60] The A−CN−K diagram is often used to reflect the degree of weathering and

https://doi.org/10.1021/acsomega.3c03144
ACS Omega 2023, 8, 26458−26478

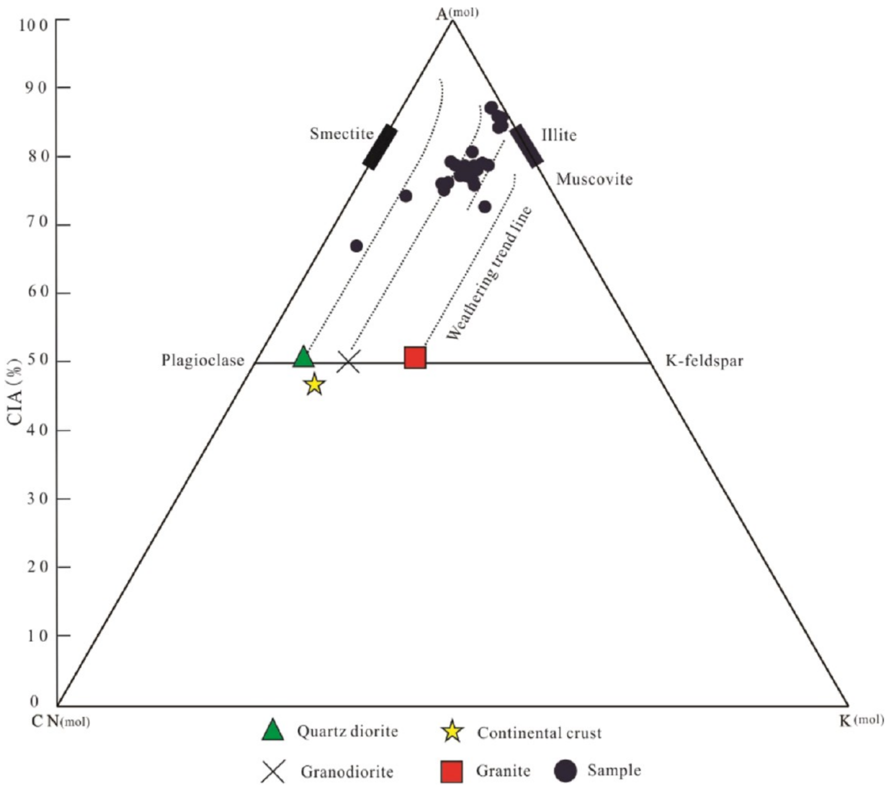

Figure 8. A−CN−K diagram of fine-grained clastic rocks of the Paleogene Gongjue Formation in the Qamdo Basin.[65]

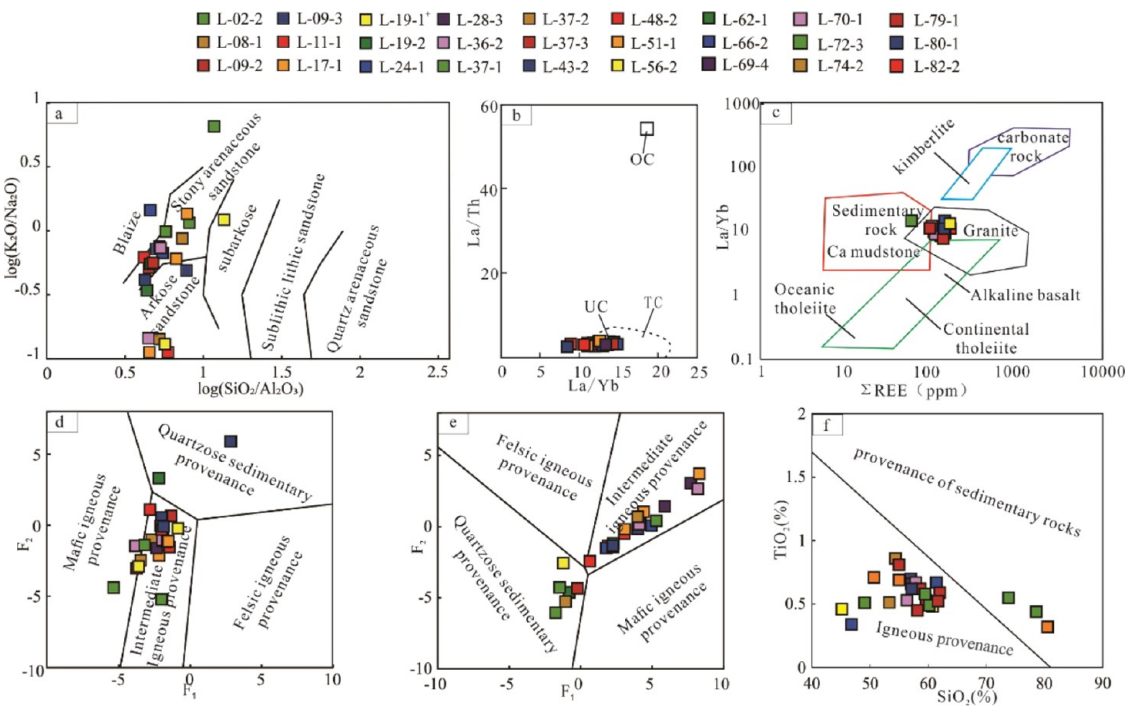

Figure 9. Discrimination diagrams showing the provenance of fine-grained clastic rocks of the Paleogene Gongjue Formation in the Qamdo Basin (Bhatia and Crook[45]). (a) $\log(K_2O/Na_2O)$ vs $\log(SiO_2/Al_2O_3)$ (from Pettijohn et al.[70]). (b) La/Th vs La/Yb (from Shao and Stattegger[71]). (c) La/Yb-ΣREE (from Bhatia[44]). (d,e) F2 vs F1 (from Roser and Korsch[72]). (f) TiO_2 vs SiO_2 (from Roser and Korsch[72]).

the effect of diagenesis or metasomatism on the samples. It is generally believed that the heavier the weathering of the provenance is, the higher the CIA value (80−100). Deviation of the CIA of the samples from the ideal weathering trend line (Figure 8, dotted curve) in the A−CN−K diagram (parallel to the A−CN axis) indicates that the samples have been affected by diagenesis and potassium metasomatism. The more significant the deviation is, the more significant the effect of potassium metasomatism.[59,60] The CIA values of the samples from the Gongjue Formation in the Qamdo Basin fall near the ideal

https://doi.org/10.1021/acsomega.3c03144
ACS Omega 2023, 8, 26458−26478

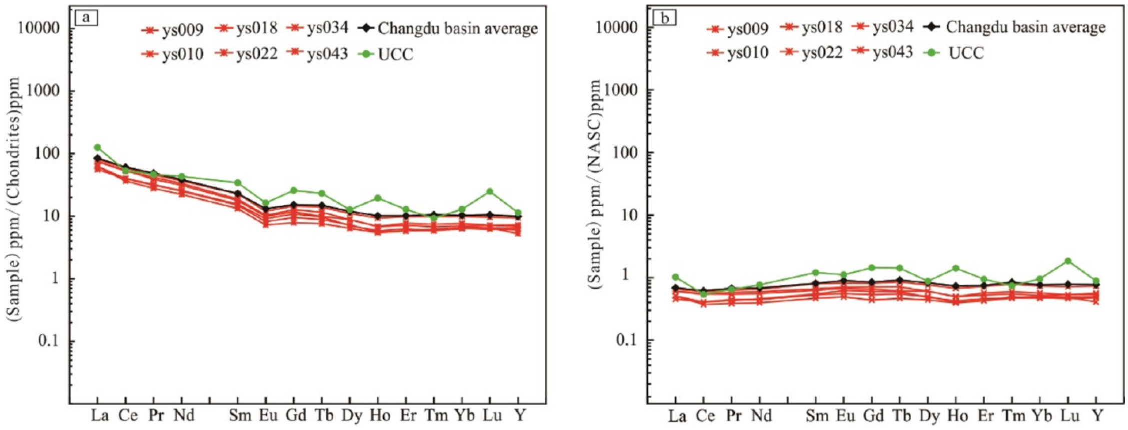

Figure 10. Chondrite- and NASC-normalized REE patterns of fine-grained clastic rocks of the Paleogene Gongjue Formation in both Qamdo Basin and Nangqian Basin. (a) Standardized chondrite curves of fine clastic rocks from the Nangqian and Qamdo basins (the samples named no. ys are from Du et al.[75] and Sun and McDonough[37]); (b) normalized curve of fine clastic rock balls in the Nangqian and Qamdo basins in North America (the samples named no. ys are from Du et al.[75] and Haskin and Paster[38]).

weathering trend line (Figure 8), indicating that the provenance was not affected by weak potassium metasomatism. At the same time, the K_2O contents (0.44−2.18%, avg. of 1.49%) of the samples are significantly lower than upper crust (2.80%),[61] which also indicates that the sediments in the provenance area were not affected by potassium metasomatism. It is evident that the CIA can effectively determine the weathering degree of the provenance area. Overall, the ICV values of 24 samples are greater than 1, while the ICV values of only 3 samples are less than 1 (0.93, 0.87, and 0.87) (Table 1), indicating that the fine-grained clastic rocks contain little clay material and indicate initial deposition in an active tectonic zone. Therefore, CIA is a reliable indicator of the chemical weathering process. The expressions of CIA, CIW (chemical index of weathering), and ICV are given by CIA = molar $[(Al_2O_3)/(Al_2O_3 + CaO^* + Na_2O + K_2O)] \times 100$, CIW = $[Al_2O_3/(Al_2O_3 + CaO^* + Na_2O)] \times 100$, and ICV = $(Fe_2O_3 + K_2O + Na_2O + CaO + MgO + MnO + TiO_2)/Al_2O_3$, respectively, where CaO* represents the CaO content in silicate minerals only.[62] In such a case, it is necessary to correct the measured CaO content in the presence of carbonates (calcite and dolomite) and apatite. In this study, the CaO content was initially corrected for phosphates using available P_2O_5 data (CaO* = mole CaO − mole $P_2O_5 \times 10/3$). If the remaining mole number was less than that of Na_2O, the mole value of CaO was adopted as that of CaO*; otherwise, the mole value of CaO* was assumed to be equal to that of Na_2O.[48,63,64] The CIA values of Paleocene fine-grained clastic rocks in the basin range between 67.08 and 87.24 (avg. of 78.93). Samples plot away from the feldspar endmember (Figure 8), whereas the CIW values of these rocks range from 82.27 to 95.73 (avg. of 90.10). The ICV values of these rocks range from 0.87 to 11.82 (avg. of 2.50). Both indices demonstrate that the parent rocks of sediments in the Paleocene Gongjue Formation have undergone heavy chemical weathering, which coincides with the heavy weathering in the Tibetan Plateau, the world's highest continental plateau.

Major oxides can also be used as a criterion for the classification and compositional maturity of sedimentary rocks. For instance, the SiO_2 content in bulk rocks is mainly dependent on the quartz content, while the whole-rock Al_2O_3 content corresponds to the contents of clay minerals and feldspars. Therefore, the SiO_2/Al_2O_3 ratio is a typical assessment index for the maturity of components.[66] In this study, the SiO_2/Al_2O_3 ratios of Gongjue fine-grained clastic rocks range between 5.93 and 7.22 (avg. of 6.02), and as all ratios are greater than 5, this indicates that these Paleocene sedimentary rocks in the Qamdo Basin have high maturity.[67] The $\log(K_2O/Na_2O)$ vs $\log(SiO_2/Al_2O_3)$ discriminant diagram shows that our samples plot within the region of feldspars and arenaceous sandstones (Figure 9a). Moreover, microscopic observations reveal that quartz and feldspars are the dominant mineral assemblages (Figure 4a−d), signifying that the fine-grained clastic rocks of the Paleocene Gongjue Formation are dominated by stony arenaceous sandstones and arkoses, with small amounts of graywackes.

The fine-grained clastic rocks of the Gongjue Formation that are plotted in the La/Th vs La/Yb diagram are mostly near the average value of continental crust (Figure 9b). In the La/Yb vs ΣREE diagram, the samples mainly plot within or near the ranges of the granite region and sedimentary rock region (Figure 9c). Based on the discriminant indices (F1 and F2) for the characteristics of oxide contents (Ti, Fe, Al, Mg, K, Ca, and Na),[68] only samples L-19-2 and L-43-2 of the fine-grained clastic rocks plot within the quartz sedimentary rock region; samples L-24-1 and L-36-2 plot in the vicinity of the source areas of mafic igneous rocks, while the rest of the samples plot within the region of intermediate igneous rocks (Figure 9d). Figure 9e shows that all fine-grained clastic rock samples plot within the source areas of intermediate igneous rocks and quartzite sediments. Moreover, the samples collected from the study area basically plot within the transition region between sedimentary rocks and igneous rocks in Figure 9f. All of these results indicate that the source rocks of the Paleocene Gongjue Formation are composed of sedimentary and igneous rocks of mixed origins. The REE signatures of North American shales and chondrites (NASC) are often used to represent the REE compositional characteristics of the upper crust.[56,69] NASC and chondrite-normalized REE partitions of Gongjue fine-grained clastic rocks show a near-horizontal distribution with slight negative Eu anomalies (Figure 6), indicating that REE compositions are similar to those of North American shales and chondrites. In conclusion, the results show that the fine-grained clastic rocks of the Paleocene Gongjue Formation in the Qamdo Basin are dominated by quartzite lithic sandstones and feldspar sandstones and that their provenances are dominated by mixed source areas of weathering products of intermediate igneous rocks, igneous rocks, and sedimentary rocks with quartz,

https://doi.org/10.1021/acsomega.3c03144
ACS Omega 2023, 8, 26458−26478

Table 5. Average Trace Element Ratios of the Paleogene Gongjue Fine-Grained Clastic Rocks in the Qamdo Basin

parameters	clastic rocks of Gongjue Formation	magnesium ferric source	felsic source	Upper Crust Composition (UCC)	Lower Crust Composition (LCC)
La/Sc	3.22	0.40−1.10	2.50−16.0	2.70	0.30
Th/Sc	1.03	0.04−0.05	0.83−20.00	1.00	0.03
Cr/Th	5.48	22.00−100.00	0.50−7.70	3.30	222.00
Co/Th	1.00	7.10−8.30	0.22−1.50	0.90	33.00
data sources	in this paper	Cullers[78]		Taylor and McLennan[56]	

Table 6. Trace Element Ratios Discriminating the Sedimentary Environment for Paleogene Gongjue Clastic Rocks in the Qamdo Basin

formation	unit	sample no.	Sr/Ba	Sr/Cu	V/Cr	U/Th	UCC-Mo_{EF}	UCC-U_{EF}	PASS-Mo_{EF}	PASS-U_{EF}
E	Eg^3	L-08-1	0.52	8.29	2.14	0.22	0.07	0.04	0.13	0.10
		L-09-2	0.45	5.29	1.16	0.26	0.05	0.07	0.09	0.09
		L-09-3	0.60	4.72	1.39	0.24	0.11	0.08	0.21	0.07
		L-11-1	0.14	15.00	1.24	0.22	0.06	0.10	0.12	0.06
		L-19-1+	0.90	8.30	0.85	0.32	0.09	0.07	0.18	0.09
		L-19-2	0.68	12.21	1.31	0.30	0.13	0.06	0.25	0.09
		L-24-1	0.22	5.62	1.48	0.32	0.08	0.05	0.15	0.04
		L-28-3	0.46	5.82	1.47	0.17	0.12	0.06	0.23	0.06
		L-72-3	0.58	7.38	0.98	0.28	0.08	0.05	0.16	0.05
		L-74-2	0.69	7.35	1.35	0.25	0.13	0.06	0.25	0.17
		L-79-1	0.44	3.61	1.48	0.27	0.07	0.07	0.13	0.09
		L-80-1	0.25	2.73	1.32	0.26	0.06	0.06	0.12	0.09
		L-82-2	0.69	3.62	1.34	0.25	0.04	0.06	0.07	0.07
	Eg^2	L-37-1	0.66	23.37	1.53	0.26	0.06	0.05	0.11	0.07
		L-37-2	0.27	1.06	1.89	0.31	0.28	0.04	0.54	0.05
		L-37-3	0.76	12.99	1.56	0.29	0.14	0.15	0.27	0.08
		L-43-2	3.69	83.78	1.70	0.33	0.11	0.08	0.20	0.09
		L-66-2	0.59	3.96	1.51	0.29	0.15	0.08	0.29	0.11
		L-69-4	0.74	6.10	1.60	0.28	0.28	0.07	0.52	0.08
		L-70-1	0.41	9.14	1.41	0.26	0.02	0.06	0.04	0.07
	Eg^1	L-02-2	0.38	5.12	0.76	0.29	0.05	0.09	0.10	0.06
		L-17-1	0.24	5.31	1.20	0.22	0.08	0.08	0.16	0.07
		L-48-2	0.31	2.91	1.37	0.24	0.09	0.06	0.17	0.06
		L-51-1	0.63	14.02	1.19	0.21	0.09	0.05	0.18	0.06
		L-36-2	0.86	14.34	1.51	0.20	0.08	0.08	0.15	0.07
		L-56-2	0.48	8.73	1.25	0.20	0.09	0.08	0.16	0.07
		L-62-1	0.90	6.90	1.19	0.26	0.05	0.04	0.09	0.06

and the minor addition of mantle-derived materials (i.e., basalt or gabbro).

In comparison, both the fine-grained clastic rocks of the Paleocene Gongjue Formation in the Qamdo Basin and those in the Nangqian Basin are dominated by red sandstones and gypsum rocks with ripple marks and multidirectional paleocurrents. The Paleocene Gongjue Formation is believed to be a set of mudstone and sandstone deposits with alluvial fan continental facies and fluvial−lacustrine facies,[73−76] which are similar to the sedimentary facies and are coincident with the tectonic setting of the Gongjue Formation in the northern Nangqian Basin that formed in a continental arc environment and passive continental rim.[20,37,41,77,78] Such a similarity in the Paleocene Gongjue Formation between the Qamdo Basin and the Nangqian Basin is also indicated by whole-rock geochemistry, such as negative Eu anomalies and LREE−HREE fractionation (Figure 10a). The NASC-normalized REE patterns of Gongjue fine-grained clastic rocks in both basins are almost parallel, horizontal, and flat (Figure 10b), indicating that the crust is the provenance of the Gongjue Formation in the two basins. In combination with the results from the La/Th vs La/Yb diagram and the average ratios of La/Sc, Th/Sc, Cr/Th, and Co/Th (Table 5), it can be inferred that the Gongjue Formation mainly originated from the upper crustal felsic source region.

5.4. Paleosalinity. The Tibetan Plateau experienced a thermal event in the Paleogene,[39] when the dry and hot climate was favorable for enrichment of elements such as Ca, Mg, K, Na, Sr, and Ba.[20,42] Therefore, these elements can often be used for reconstructing paleoclimatic conditions.[20,40,43] The Sr/Ba ratio is generally used to evaluate the salinity in sedimentary water whereby Sr/Ba > 0.5 in sediments indicates marine water, Sr/Ba < 0.2 indicates freshwater, and 0.2 < Sr/Ba < 0.5 indicates brackish water.[38,79] Sr/Ba ratios of fine-grained clastic rocks in the Gongjue Formation are mostly concentrated within the interval of 0.14 to 0.90 (Table 6), indicating brackish to marine paleowater conditions during deposition of this stratum in the Paleogene (Figures 11 and 12a). The water salinity in the lacustrine system during the deposition of the Gongjue Formation is consistent with the occurrence of gypsum in this stratum (Figure 3e,f). The brackish to saline water mass in the paleolake during deposition of the Gongjue Formation intensely evaporated during the late stage of the Qamdo Basin evolution, representing a shrinkage stage of this lacustrine system, which

https://doi.org/10.1021/acsomega.3c03144
ACS Omega 2023, 8, 26458−26478

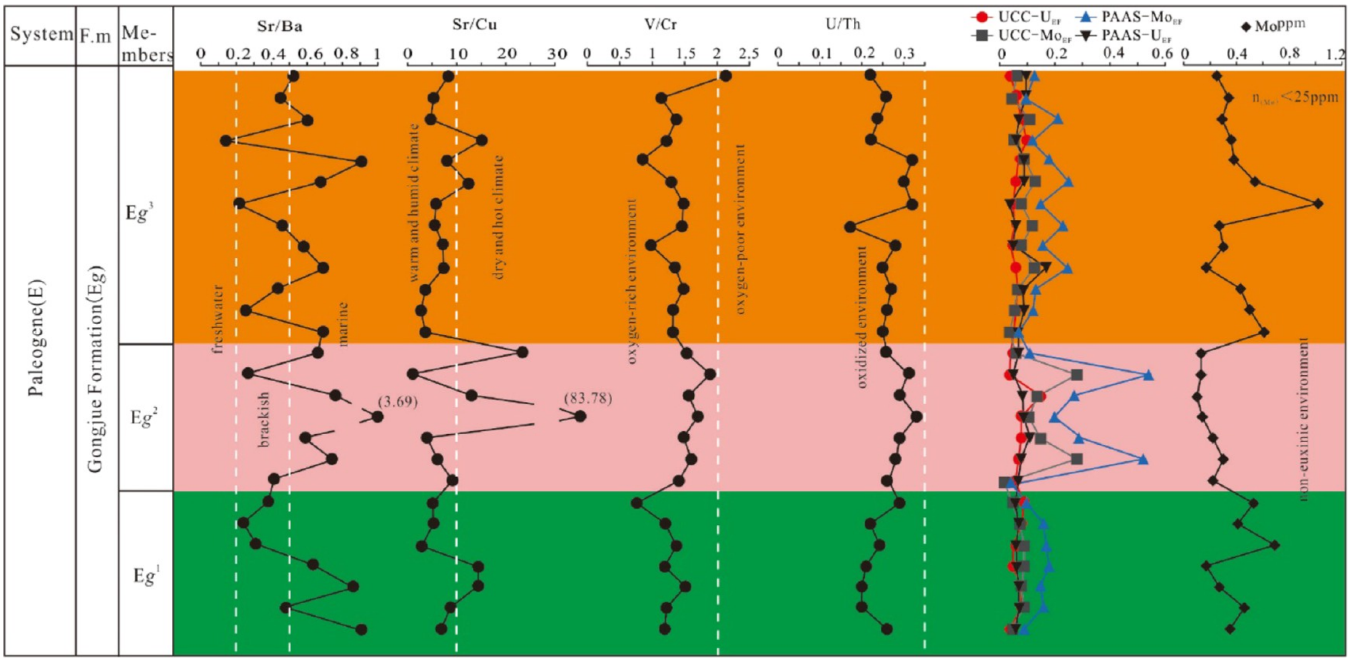

Figure 11. Evolution of the sedimentary environment of the Paleogene Gongjue Formation in the Qamdo Basin.

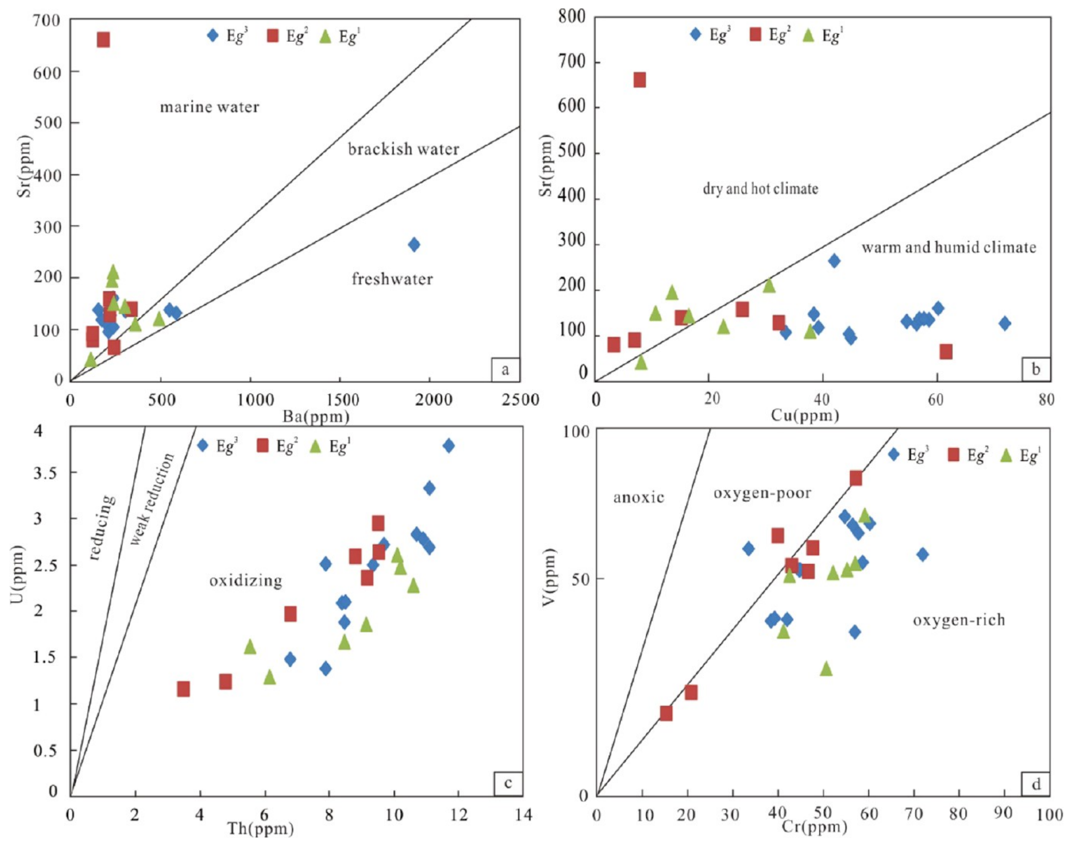

Figure 12. Cross plots of paleoclimate (Sr/Cu), paleosalinity (Sr/Ba), and redox (Th/U and V/Cr) contents of samples from the Paleogene Gongjue Formation in the Qamdo Basin. (a) Paleosalinity scatter plot of Sr and Ba elements. (b) Paleoclimate scatter plot of Sr and Cu elements. (c) Scatter plot of the redox conditions of U and Th elements. (d) Scatter plot of the oxygen degree of V and Cr elements.

might have resulted from collision between the Tibetan and Indian plates.[80−83]

5.5. Redox Conditions. The V/Cr ratio is sensitive to variation in redox conditions. V/Cr < 2.0 denotes an oxygen-rich environment, 2.00 < V/Cr < 4.25 implies an oxygen-poor environment, and V/Cr > 4.25 indicates an oxygen-poor to anoxic environment.[20,50,84] V/Cr ratios in the Gongjue Formation are mostly less than 2.0 but are exceptionally higher than 2.0 for one sample in the middle Gongjue Formation (Table 4). This suggests oxidizing conditions during the

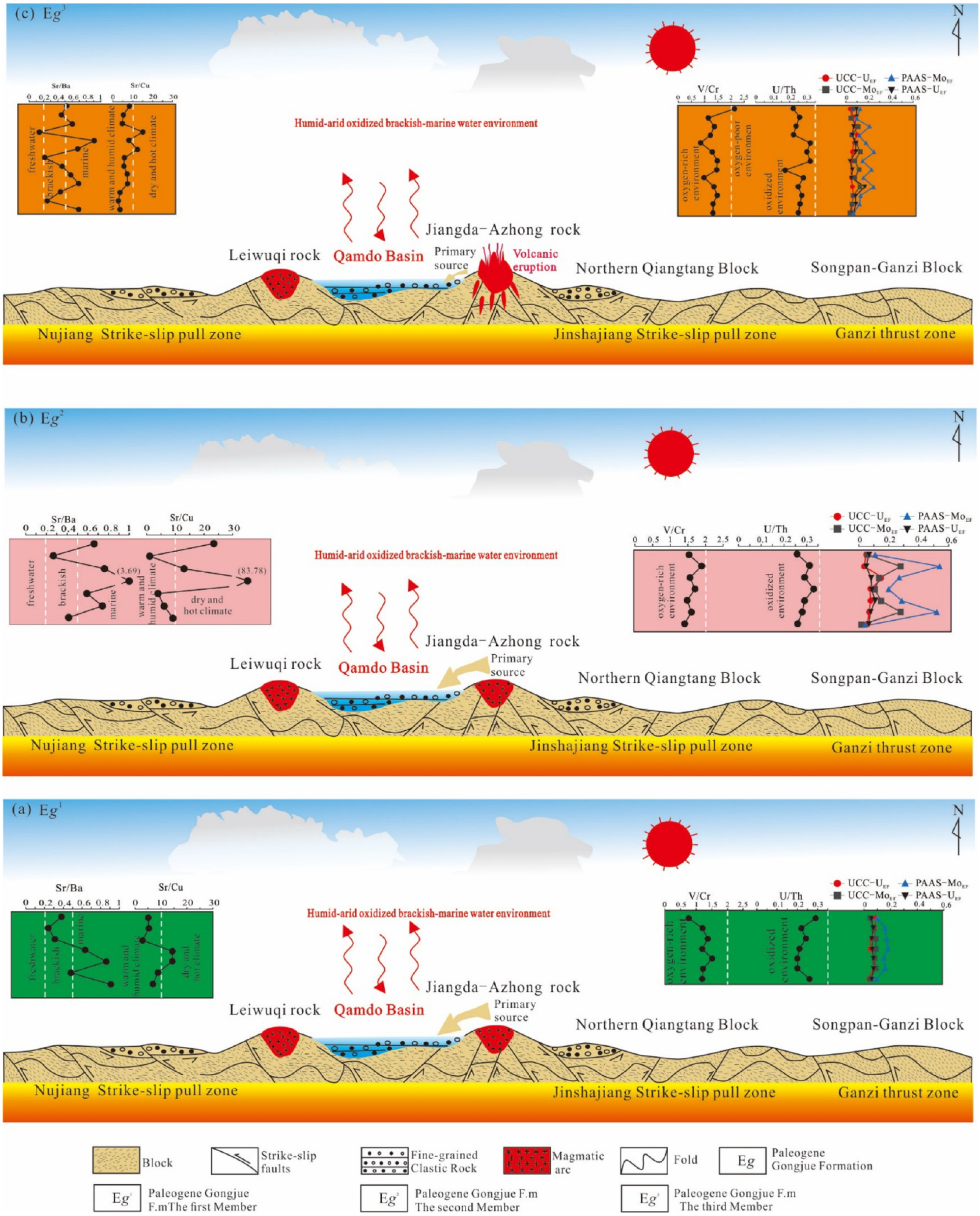

Figure 13. Sedimentary environment evolution model of the three members of the Paleocene Gongjue Formation in the Qamdo Basin: (a) Eg^1, (b) Eg^2, and (c) Eg^3.

https://doi.org/10.1021/acsomega.3c03144
ACS Omega 2023, 8, 26458−26478

deposition of the Gongjue Formation and probably reducing conditions in the middle Gongjue Formation (Figures 11 and 12c).

The U/Th ratio can be applied to deduce the redox conditions for water bodies. U/Th > 1.25 indicates strongly reducing conditions, U/Th ratios between 0.75 and 1.25 indicate reducing conditions, and U/Th < 0.75 indicates oxidizing conditions.[20,50,84] All U/Th ratios in the Gongjue Formation are less than 0.75 (Table 4), suggesting an oxidizing paleowater environment during deposition of this stratum (Figure 11). However, the U/Th profile upsection shows a higher U/Th ratio in the middle Gongjue Formation than in the lower and upper parts of the Gongjue Formation, suggesting a lower oxygen concentration during deposition of the middle Gongjue Formation (Figure 12d), consistent with the V/Cr ratios (see immediately above).

Mo and U elements are very low in phytoplankton, and their sedimentary enrichment is generally derived from autogenic enrichment. In oxidized seawater, Mo exists in the form of stable and inactive molybdate ions (MoO_4^{2-}). Given the very limited accumulation of authigenic Mo in an oxidized environment, the concentration of seabed sediments in the modern continental rim is as low as 1−5 ppm.[85−87] Under anoxic−sulfur-rich conditions, a specific concentration of hydrogen sulfide (approximately 50 to 250 μM) is capable of activating Mo, thereby catalyzing the conversion of molybdate into thiomolybdate ($(MoO_xS_{(4-x)})^{2-}$, $x = 0-3$),[46,47,85,88] and the latter is easily deposited with sulfurized organic matter or iron sulfides.[89−92] Under oxidized conditions, U exists in the primary form of soluble hexavalent uranyl carbonate complexes and shows chemical inertness.[93−97] The enrichment of authigenic U is relatively limited in an oxidizing environment, and the U concentrations are only ∼1−5 ppm in seabed sediments of the modern continental rim.[56,98,99] Under anoxic conditions, hexavalent U(VI) is reduced into tetravalent U(IV) in the possible form of insoluble uranyl ions UO^{2+} or weakly soluble uranyl fluoride complexes. Therefore, the above chemical properties of Mo and U show that they can be used to evaluate the redox conditions of ancient waters. Studies before 2000 mainly analyzed the original concentrations and the ratios between these two elements,[48] while recent studies tend to use the standardized enrichment coefficient of Al to evaluate the redox conditions of ancient waters.[100−102] The formula for calculating the enrichment coefficient is given by

$$X_{EF} = (X/Al)_{sample}/(X/Al)_{UCC\ or\ PAAS}$$

where X and Al represent the mass concentrations of elements X and Al (ppm), respectively. The samples are generally standardized using upper continental crust (UCC) rocks[103] or post-Archean average shales (PAAS) from Australia.[56] U/Al_{UCC} is 0.35×10^{-4}, and Mo/Al_{UCC} is 0.19×10^{-4}; the values of U/Al_{PAAS} and Mo/Al_{PAAS} are 0.31×10^{-4} and 0.10×10^{-4}, respectively.[48] An element has good autogenetic enrichment if its enrichment coefficient is greater than 3 and less than 10 or large-scale autogenetic enrichment if its enrichment coefficient is greater than 10.

Based on the Mo and U contents in fine-grained clastic rock samples of the Gongjue Formation in the Qamdo Basin, the enrichment coefficients of Mo and U were calculated using the UCC and PAAS of Australia. The Mo_{EF} and U_{EF} values of the UCC and PAAS are less than 0.2 in the lower and upper Gongjue Formation but higher than 0.2 in the middle Gongjue Formation (Figure 11). This suggests that redox conditions of the paleowater mass in the middle Gongjue Formation were less oxidizing than those in the lower and upper Gongjue Formation. However, all Mo_{EF} and U_{EF} values are less than 1 in the entire Gongjue Formation (Table 4), indicating oxic conditions. These conclusions may be related to the shallow lacustrine water depths, which were influenced by lake waves.

According to the compiled database of modern marine systems, Mo concentrations below 25 ppm usually represent a noneuxinic environment: those with 25−100 ppm usually represent intermittent euxinia, and those with more than 100 ppm usually represent persistent euxinia.[104] The Mo content of the fine-grained rocks of the Gongjue Formation in the Chamdo Basin is less than 25 ppm(Table 2), indicating that the Gongjue Formation formed in an oxidizing environment (Figure 11).

In summary, the Gongjue Formation is generally formed in an oxic environment, with brackish to marine water and a climate consisting of a cyclical cycle of warm and humid to dry and hot.

5.6. Provenance−Sedimentary−Environment Model.

Intracontinental convergence of the Qamdo Basin was mainly the result of collision between the Indian and Eurasian plates. The idea that the collision occurred during the Late Cretaceous−Eocene is corroborated by multiple models of single-stage and multistage collision.[32,91,105,106] Such a collisional effect led to the stratified disengagement and slippage of crust and lithosphere due to large-scale thrust nappes, strike-slip pull-apart tectonics, and thrusting and stretching effects caused by intracontinental orogenesis in the Qamdo Basin, thereby forming a series of strike-slip pull-apart basins (Figure 13).[1] Within the Qamdo Basin, a depositional system of lacustrine−fluvial facies developed, and a set of red clastic rocks of the Gongjue Formation were deposited. Afterward, due to continuous subduction of the Indian plate under the Eurasian plate, the collisional effect continued to intensify in the area, forming a series of mountain system superimpositions and restructurings and dramatic thickening of the crust; thus, the Nujiang thrust belt, Taniantaweng erosional belt, Jinshajiang fold-and-thrust belt, and Ganzi fold-and-thrust belt subsequently formed.[1] In addition, beginning 65 Ma ago, the collision of the Indian-Asian continent with the Qamdo Basin resulted in the formation of a series of thrust-nappe structures in the central, northern, and eastern regions of the Qinghai Tibet Plateau, and the Qamdo contracted to form a foreland basin. During sedimentation of the Gongjue Formation, the first and second sections primarily evolved from lake facies to river facies and were deposited as mudstone and limestone (Figure 13a,b). In contrast, large-scale strike-slip stretching developed in the north and east of the Qinghai Tibet Plateau during the third sedimentation interval of the Gongjue Formation (Eg^3), transforming some early Foreland basins into pull-apart basins where a suite of red lacustrine mudstone and gypsum deposits (Eg^3) were deposited alongside widespread volcanic activities (Figure 13c). Based on the $\log(Na_2O/K_2O)-\log(SiO_2/Al_2O_3)$, La/Th−La/Yb, La/Yb−∑REE, F2−F1, and TiO_2-SiO_2 diagrams of elements of the fine-grained clastic rocks of the Gongjue Formation, its provenance is dominated by intermediate−acidic volcanic rocks, and the tectonic background diagram reveals a mainland continental arc environment. Furthermore, Bian et al.[107] suggested that the U−Pb ages of detrital zircon in the Gongjue Formation, Qamdo Basin mainly cluster around 200−350 and 350−500 Ma. This corresponds to the Mesozoic volcanic eruption (∼205 Ma) and metamorphic zircon record in the North Qiangtang Terrane, the extensively distributed Indonesian granite (205−243 Ma) and sedimentary recycling material in the Songpan-Ganzi Terrane. Therefore, the source of fine-grained clastic rocks in the Gongjue Formation of the Qamdo Basin mainly originates from the eastern part of the Northern Qiangtang Terrane and the Songpan-Ganzi Terrane (Figure 13).

The Gongjue Formation of the Qamdo Basin is divided into four sections: Eg^1, Eg^2, Eg^3, and Eg^4. Sr/Ba, Sr/Cu, V/Cr, U, Th, and U_{EF}−Mo_{EF} characteristics in the fine-grained clastic rocks of the Gongjue Formation indicate that the environment of Eg^1, Eg^2, and Eg^3 is oxidized (Figure 13). Among the three sections, Eg^1 and Eg^3 show similar U_{EF}−Mo_{EF} characteristics (Figure 13a,c), while Eg^2 displays a clear enhancement-diminution-enhancement trend (Figure 13b). From Eg^1 to Eg^3, the water column salinity and climate vary significantly. The initial water column in Eg^1 consists of seawater-brackish water-seawater-brackish water, which is compatible with the changing climate from warm-humid to dry and then back to warm-humid. This reflects the following process: (1) an arid and hot environment that enhances the evaporation of the initial water column in Eg^1, with a seawater-like salinity, and (2) diminished evaporation contributes to the formation of wet, brackish water column in Eg^1. In contrast, Eg^2 begins with a warm-humid, dry-hot climate, with the water column shifting from a brackish water environment of Eg^1 to a saline environment of seawater, after which the climate changes to a warm-humid-dry climate, with the water column shifting from brackish water to seawater. The water column salinity and climate change from Eg^1 to Eg^3 in the Gongjue Formation are large. The water column of the Gongjue Formation starts at Eg^1 with a seawater-brackish water-seawater-brackish water, while the climate changes from warm-humid-dry-warm-humid (Figure 13a), reflecting a dry-hot climate with increased evaporation and water column salinity characteristic of seawater at the start of Eg^1, followed by a humid, brackish water column with reduced evaporation intensity. The Eg^2 of the Gongjue Formation begins with a warm-humid-dry-hot climate, with the water column shifting from a brackish water environment of Eg^1 to a saline environment of seawater. Subsequently, the climate changes to a warm-humid-dry climate, with the water column shifting from brackish water to seawater (Figure 13b), probably due to the input of freshwater from the surrounding area or a decrease in atmospheric precipitation, reflecting the frequent change from humid-dry-hot climate of Eg^2, with the salinity of the water column also undergoing frequent changes. At the beginning of Eg^3 in the Gongjue Formation, the humid climate water column maintained the seawater environment of Eg^2, followed by a brackish water-seawater water column, and by the time the climate in the upper part of Eg^3 changed from humid-dry and hot, the water column also changed with the change from brackish water-seawater (Figure 13c). This reflects the change in climate from humid-dry in Eg^3 and also from brackish water- seawater water with no frequent change in climate relative to Eg^2, without frequent changes. Overall, the climate of the Gongjue Formation in the Qamdo Basin changes frequently from a warm-humid climate to a dry-hot climate, and similarly, the salinity of the water column changes from brackish water to seawater, particularly in Eg^2 where the salinity of the climate and water column salinity changes more frequently. This change in climate and water column salinity may be related to the Paleocene−Eocene maximum heat event, which resulted in a global temperature increase of 5−10 °C and atmospheric humidity.[108,109] Thus, changes in climate during the Paleocene Gongjue period in the Qamdo Basin of the Tibetan Plateau are a response to global Paleocene−Eocene climate change.

6. CONCLUSIONS

(1) Sr/Ba, Sr/Cu, V/Cr, U/Th, CIA, CIW, Mo_{EF}, and U_{EF} ratios shown in the fine-grained clastic rocks of the Paleocene Gongjue Formation indicate that the first, second, and third members of the formation experienced periodic and significant environmental and climatic changes. Overall, the Paleocene Gongjue Formation contains brackish-to-marine water facies that was deposited in an oxidized environment under a dry and hot climate, which subsequently underwent heavy weathering.

(2) Based on normalized trace elements and REE patterns of the fine-grained clastic rocks of the Gongjue Formation in combination with the $\log(Na_2O/K_2O)$ vs $\log(SiO_2/Al_2O_3)$, La/Th−La/Yb, La/Yb−ΣREE, F2−F1, and TiO_2−SiO_2 diagrams, these rocks are mainly composed of lithic sandstones and feldspathic sandstones, which have undergone severe weathering. These rocks mainly stem from the quartz weathering products of intermediate igneous rocks and sedimentary rocks of the upper crust.

(3) Based on the structural background and sedimentary environment characteristics of the La−Th, Th−Sc−Zr/10, Th−Co−Zr/10, and La−Th−Sc plots and Sr/Ba, Sr/Cu, V/Cr, U, Th, and U_{EF}−Mo_{EF}, together with results from the literature pertaining to the tectonic evolution and formation time period of the basin, the provenance of the red Paleocene Gongjue Formation in the Qamdo Basin is likely derived mostly from the eastern part of the Northern Qiangtang block and Songpan-Ganzi block.

■ ASSOCIATED CONTENT

Data Availability Statement

All data generated or analyzed during this study are included in this article.

■ AUTHOR INFORMATION

Corresponding Authors

Zhibo Zhang − *School of Resources and Geosciences, China University of Mining and Technology, Xuzhou, Jiangsu 221116, China*; orcid.org/0000-0002-7140-1253; Email: zzb397132190@126.com

Huan Li − *School of Geosciences and Info-Physics, Central South University, Changsha 410083, China*; Email: lihuan@csu.edu.cn

Authors

Weiqing Zheng − *Environmental Science and Technology Company Limited, No.1 Bureau of CMGB, Xiongan, Hebei 071700, China*

Scott A. Whattam − *Department of Geosciences, King Fahd University of Petroleum and Minerals, Dhahran 31261, Saudi Arabia*

Zhijun Zhu − *Department of Geosciences, School of Earth Sciences, East China University of Technology, Nanchang, Jiangxi 330013, China*

Weicheng Jiang − *Department of Earth and Environmental Sciences, Macquarie University, Sydney, NSW 2109, Australia*

Difei Zhao − *School of Resources and Geosciences, China University of Mining and Technology, Xuzhou, Jiangsu 221116, China*

Complete contact information is available at:

https://doi.org/10.1021/acsomega.3c03144
ACS Omega 2023, 8, 26458−26478

https://pubs.acs.org/10.1021/acsomega.3c03144

Author Contributions

Conceptualization, Z.Zhang; methodology, Z.Zhang, H.L., and Z.Zhu; software, S.A.W. and W.Z.; validation, W.J., D.Z.; formal analysis, Z.Zhang; investigation, Z.Zhang; resources, Z.Zhang and Z.Zhu; data curation, Z.Zhang; writing—original draft preparation, Z.Zhang and S.A.W.; writing—review and editing, H.L. and Z.Zhang; visualization, Z.Zhang and W.J.; supervision, H.L.; project administration, H.L.; funding acquisition, H.L.

Notes

The authors declare no competing financial interest.

■ ACKNOWLEDGMENTS

We thank Heng-ye Wei, Professor Xiu-gen Fu, and Professor Liu-Qin Chen for their encouragement and constructive comments on the manuscript. We would also like to thank the anonymous reviewers for their comments that helped to improve the manuscript. This work was supported by the Jiangsu Natural Science Foundation project (Grant No. SBK2021045820), the Chongqing Natural Science Foundation general Project (Grant No. cstc2021jcyj-msxmX0624), the Graduate Innovation Program of China University of Mining and Technology (Grant No. 2022WLKXJ002), and the Postgraduate Research & Practice Innovation Program of Jiangsu Province (Grant No. KYCX22_2600). S.A.W. acknowledges KFUPM for funds from Project Nos. SF18068 and SF18069.

■ REFERENCES

(1) Geological Survey Institute of Tibet Autonomous Region *Nangqian County-Chandu County-Jiangda County Regional Geological Survey Report*; Geological, Survey Special Report, in Chinese with report, 2007.

(2) Jiang, Q.-Y.; Li, C.; Su, L.; Hu, P.-Y.; Xie, M.-C.; Wu, H. Carboniferous Arc Magmatism in the Qiangtang Area, Northern Tibet: Zircon U-Pb Ages, Geochemical and Lu-Hf Isotopic Characteristics, and Tectonic Implications. *J. Asian Earth Sci.* **2015**, *100*, 132−144.

(3) Song, P.; Ding, L.; Li, Z.; Lippert, P. C.; Yue, Y. An early bird from Gondwana: Paleomagnetism of Lower Permian lavas from northern Qiangtang (Tibet) and the geography of the Paleo-Tethys. *Earth Planet. Sci. Lett.* **2017**, *475*, 119−133.

(4) Xu, Y. *Analysis of Paleogene Sedimentary Characteristics in Changdu Basin, Tibet*; Nanchang, East China University of Technology in Chinese with thesis, 2020.

(5) Xiao, R.Y. *Magnetic stratigraphy of Gongjue Basin in the southeastern margin of Qinghai-Tibet Plateau and its Sediment-tectonic implications*; Nanjing Normal University in Chinese with thesis: Nanjing, 2021.

(6) Wang, J.; Fu, X.; Wei, H.; Shen, L.; Wang, Z.; Li, K. Late Triassic basin inversion of the Qiangtang Basin in northern Tibet: Implications for the closure of the Paleo-Tethys and expansion of the Neo-Tethys. *J. Asian Earth Sci.* **2022**, *227*, No. 105119.

(7) Jiang, Y. B.; Hou, Z. Q.; Yan, Z. B.; Du, H. F.; Guo, F. S.; Liu, Y. X. Prototype and evolution of the Tertiary Basins in Yushu Area Qinghai. *Geotecton. Metallog.* **2009**, *33*, 521−529. in Chinese with English abstract.

(8) Yang, K.; Mo, X. Late Paleozoic Rifting-related Volcanic Rocks and Tectonic Evolution in Southwestern Yunnan. *Acta Petrol. Mineral.* **1993**, 297−311.

(9) Zhu, L.; Zhang, H. H.; Wang, J. H.; Zhou, J. Y.; Xie, G. H. 40Ar /39Ar Chronology of High-K Magmatic Rocks in Nangqian Basins At The Northern Segment of the Jinsha- Red River Shear Zone (JRRSZ). *Geotecton. Metallog.* **2006**, *30*, 241−247. in Chinese with English abstract.

(10) Deng, W. M.; Sun, H. J.; Zhang, Y. Q. K-Ar Age of Cenozoic volcanic rocks in Nangqian Basin, Qinghai Province. *Chin. Sci. Bull.* **1999**, *23*, 2554−2558. in Chinese with thesis.

(11) Wei, M. Neogene ostracism of Nangqian, Qinghai. *Geological Collection of Qinghai-Tibet Plateau*; Beijing, Geological Publishing House, 1985, no. *17*, pp. 313-325. in Chinese with thesis.

(12) Zhou, J.; Wang, J.; An, Y.; Horton, B. K.; Spurlin, M. S. Sedimentology and Tectonic Significance of Paleogene Coarse Clastic Roeks in Eastern Tibet. *Acta Geol. Sin.* **2003**, *77*, 262−271. in Chinese with English abstract.

(13) Zhang, K. X.; Wang, G. C.; Chen, F. N.; Xu, Y. D.; Luo, M. S.; Xiang, S. Y.; Kou, X. H.; Zhao, L. S. Coupling between the Uplift of Qinghai-Tibet Plateau and Distribution of Basins of Paleogene-Neogene. *Earth Sci.* **2007**, *32*, 583−597. in Chinese with English abstract.

(14) Jiang, Y. B.; Hou, Z. Q.; Yan, Z. B.; Du, H. F.; Guo, F. S.; Liu, Y. X. Prototype and evolution of the Ttertiary Basins in Yushu Area Qinghai. *Geotecton. Metallog.* **2009**, *33*, 521−529. in Chinese with English abstract.

(15) Horton, B. K.; Zhou, J. Y.; Spurlin, M. S.; Wang, J. H. Paleogene deposystems and basin evolution in the eastern Tibetan Plateau: Nangqian and Xialaxiu Bains. *Earth Sci. Front.* **2000**, *7*, 282−283. in Chinese with English abstract.

(16) Wang, S. F.; Yi, H. S.; Wang, C. S. Sedimentary features of the Nangqian tertiary basin in Qinghai Province. *J. Chengdu Univ. Tech. (Sci. Tech. Edition)* **2001**, *28*, 13−16. in Chinese with English abstract.

(17) Zhou, J. Y.; Wang, J. H.; An, Y.; Horton, B. K.; Spurlin, M. S. Depositional Patterns and Tectonic Setting of Early Tertiary Basins in the NE Margin of the Tibetan Plateau: A Case Study of the Nangqian and Xialaxiu Basins. *Acta Sedimentol. Sin.* **2002**, *20*, 85−91. in Chinese with English abstract.

(18) Zhang, Z. B.; Xu, Y.; Miao, Y. J.; Wang, W. F.; Zhao, D. F.; Chen, L. D. Provenance and Sedimentary Environment of Paleogene Gongjue Formation in Qamdo Basin. *Acta Sedimentol. Sin.* **2022**, *40*, 1561−1581. in Chinese with English abstract.

(19) Cao, W.; Yan, D.-P.; Qiu, L.; Zhang, Y.; Qiu, J. Structural style and metamorphic conditions of the Jinshajiang metamorphic belt: Nature of the Paleo-Jinshajiang orogenic belt in the eastern Tibetan Plateau. *J. Asian Earth Sci.* **2015**, *113*, 748−765.

(20) Zhang, Z. B.; Zhu, Z. J.; Li, H.; Jiang, W. C.; Wang, W. F.; Xu, Y.; Li, L. R. Provenance and salt structures of gypsum formations in Pb-Zn ore-bearing Lanping basin, Southwest China. *J. Cent. South. Univ.* **2020**, *27*, 1828−1845.

(21) Zhang, Z. B.; Zhu, Z. J.; Wang, W. F.; Xu, Y.; Li, L. R. Geochemical Characteristics and Formation Environment of Mesozoic and Cenozoic Evaporative Rocks in Lanping Basin, Western Yunnan. *J. Jilin Univ. (Earth Sci. Ed.)* **2019**, *49*, 356−379. in Chinese with English abstract.

(22) Pan, G. T.; Chen, Z. L.; Li, X. Z.; Yang, Y. J.; Xu, X. S.; Xu, Q.; Jiang, X. S.; Wu, Y. L.; Luo, J. N.; Zhu, T. X.; Peng, Y. M. *Geological-tectonic Evolution in the Eastern Tethys*; Geological Publishing House: Beijing, 1997. in Chinese with English abstract.

(23) Pan, Y. S. Discussion on the tectonic properties of the middle member of Bangonghu-Nujiang belt. *Chin. J. Geol.* **1983**, 139−148. in Chinese with English abstract.

(24) Li, C.; Huang, X. P.; Zhai, Q. G.; Zhu, T. X.; Yu, Y. S.; Wang, G. H.; Zeng, Q. G. The Longmu Co-Shuanghu-Jitang plate suture and the northern boundary of Gondwanaland in the Qinghai-Tibet plateau. *Earth Sci. Front.* **2006**, 136−147. in Chinese with English Abstract.

(25) Pan, G. T.; Mo, X. X.; Hou, Z. Q.; Zhu, D. C.; Wang, L. Q.; Li, G. M.; Zhao, Z. D.; Geng, Q. R.; Liao, Z. L. Spatial-temporal framework of the Lhasa orogenic belt and its evolution. *Acta Petrol. Sin.* **2006**, 521−533. in Chinese with English abstract.

(26) Li, C.; Zhai, Q. G.; Chen, W.; Dong, Y. S.; Yu, J. J. Geochronology evidence of the closure of Longmu Co-Shuanghu suture, Qinghai-Tibet plateau: Ar-Ar and zircon SHRIMP geochronology from ophiolite and rhyolite in Guoganjianian. *Acta Petrol. Sin.* **2007**, *23*, 911−918. in Chinese with English abstract.

(27) Hu, X. M. Overview of the Late Mesozoic Paleogene major paleoceanographic and geological events in Eastern Tethyan Ocean. *Chin. J. Nat.* **2015**, *37*, 93−102.
(28) Fan, J. J.; Li, C.; Wang, M.; Xie, C. M.; Xu, W. Features, provenance, and tectonic significance of Carboniferous-Permian glacial marine diamictites in the Southern Qiangtang-Baoshan block, Tibetan Plateau. *Gondwana Res.* **2015**, *28*, 1530−1542.
(29) Yan, D. P.; Zhou, Y.; Qiu, L.; Wells, M. L.; Mu, H.; Xu, C. G. The Longmenshan Tectonic Complex and adjacent tectonic units in the eastern margin of the Tibetan Plateau: A review. *J. Asian Earth Sci.* **2018**, *164*, 33−57.
(30) Yan, D. P.; Qiu, L.; Wells, M. L.; Zhou, M. F.; Meng, X. K.; Lu, S.; Zhang, S.; Wang, Y.; Li, S. B. Structural and geochronological constraints on the early Mesozoic north Longmen Shan Thrust Belt: Foreland fold-thrust propagation of the SW Qinling orogenic belt, northeastern Tibetan plateau. *Tectonics* **2018**, *37*, 4595−4624.
(31) Qiu, L.; Yan, D. P.; Yang, W. X.; Wang, J.; Tang, X.; Ariser, S. Early to Middle Triassic sedimentary records in the Youjiang Basin, South, China: Implications for Indosinian orogenesis. *J. Asian Earth Sci.* **2017**, *141*, 125−139.
(32) Tang, J. X.; Zhong, K. H.; Liu, Z. C.; Li, Z. J.; Dong, S. Y.; Zhang, L. Intracontinental Orogen and Metal- logenesis in Himalayan Epoch: Qamdo Large Composite Basin, Eastern Tibet. *Acta. Geol. Sin.* **2006**, *80*, 1364−1376. in Chinese with English abstract.
(33) Qi, Z. L. *Characteristics of the Source Rocks in Nangqian-Qamdo Area, Eastern Tibet: Implications for unconventional oil and gas re provenance, Beijing*; China University of Geosciences, 2017. in Chinese with thesis.
(34) Zuo, P. *Hydrocarbon source rock characteristics and shale gas resource potential in Qamdo basin during the upper Permian series-upper Triassic series*; Beijing, China University of Geosciences, 2016. in Chinese with thesis.
(35) He, Z. J.; Li, J. Y.; Mo, S. S.; Sorokin, A. A. Tectonic setting and provenance analysis of sandstone geochemistry in Mohe foreland basin. *Sci. China (Ser. D)* **2003**, 1219−1226.
(36) Yan, M.; Chi, Q.; Gu, T.; Wang, C. Chemical Compositions Of Continental Crust And Rocks In Eastern China. *Geophys. Geochem. Explor.* **1997**, *21*, 451−459.
(37) Sun, S. S.; McDonough, W. F. *Chemical and isotopic systematics of oceanic basalts: implications for mantle composition and processes*; Geological Society, London, Special Publications, 1989, vol. *42*, pp. 313-345.
(38) Haskin, L.A.; Paster, T.P. Chapter 21 Geochemistry and mineralogy of the rare earths. *Handbook on the Physics and Chemistry of Rare Earths*; 1979, vol. *3*, pp. 1-80.
(39) Zhao, D. J.; Wang, X. Q. Geochemical Characteristics and Prospecting Potential of the Middle Triassic Fine Clastic Rocks in Youjiang Basin. *Geotecton. Metallog.* **2020**, *44*, 311−324. in Chinese with English abstract.
(40) Huang, G.; Pan, J.; Xia, F.; Yan, J.; Zhang, C.; Wu, D.; Liu, Y. Provenance of uranium mineralization of the Yuqia area, Northwest China: Constraints from detrital zircon U-Pb geochronology and Hf isotopes. *J. Earth Sci.* **2022**, *33*, 1549−1570.
(41) Sun, J.; Dong, Y.; Ma, L.; Chen, S.; Jiang, W. Devonian to Triassic tectonic evolution and basin transition in the East Kunlun−Qaidam area, northern Tibetan Plateau: Constraints from stratigraphy and detrital zircon U−Pb geochronology. *Geol. Soc. Am. Bull.* **2022**, *134*, 1967−1993.
(42) Sun, J.; Yang, L.; Dong, Y.; Yang, X.; Peng, Y.; Zhao, J. Permian tectonic evolution of the southwestern Ordos Basin, North China: Integrating constraints from sandstone petrology and detrital zircon geochronology. *Geol. J.* **2020**, *55*, 8068−8091.
(43) Sun, J.; Dong, Y.; Chen, Q.; Yang, L.; Li, W.; Zhang, D. D.; Zhang, Q. Ordovician tectonic transition from passive margin into peripheral foreland in the southern Ordos: a diagnostic insight into the closure of Erlangping Ocean between the North Qinling Arc and North China Block. *Basin Res.* **2023**, *35*, 336−362.
(44) Bhatia, M. R. Rare earth elements geochemistry of Australian Paleozoic graywackes and mudrocks: Provenance and tectonic control. *Sediment. Geol.* **1985**, *45*, 97−113.
(45) Bhatia, M. R.; Crook, K. A. W. Trace element characteristics of graywackes and tectonic setting discrimination of sedimentary basins. *Contrib. Mineral. Petrol.* **1986**, *92*, 181−193.
(46) Wei, H.; Tang, Z.; Yan, D.; Wang, J.; Roberts, A. P. Guadalupian (Middle Permian) ocean redox evolution in South China and its implications for mass extinction. *Chem. Geol.* **2019**, *530*, No. 119318.
(47) Wei, H.; Jiang, X. Early Cretaceous ferruginous and its control on the lacustrine organic matter accumulation: Constrained by multiple proxies from the Bayingebi Formation in the Bayingebi Basin, inner Mongolia, NW China. *J. Pet. Sci. Eng.* **2019**, *178*, 162−179.
(48) Qiu, Z.; Wei, H. Y.; Liu, H. L.; Shao, N.; Wang, Y. M.; Zhang, L. F.; Zhang, Q. Elementary geochemical characteristics of extraordinarily high organic matter accumulation for unconventional petroleum sedimentology. *Oil Gas Geol.* **2021**, *42*, 91−948. in Chinese with English abstract.
(49) Tian, J. C.; Zhang, X. *Sedimentary geochemistry*; Geological Publishing House: Beijing, 2016. (in Chinese).
(50) Wang, Y. Y.; Wu, P. Geochemical criteria of sediments in the coastal area of Jiangsu and Zhejiang Provinces. *J. Tongji Univ.* **1983**, *4*, 82−90. in Chinese with English abstract.
(51) Mao, G. Z.; Liu, C. Y. Application of geochemistry in provenance and sedimentary background analysis. *J. Earth Sci. Environ.* **2011**, *33*, 33−348. in Chinese with English abstract.
(52) Zhu, Z. J.; Guo, F. S.; Song, Y. C.; An, Q. Geological Characteristics and Metallogenic Relationship of the Paleogene in Lanping Basin. *Acta Sedimentol. Sin.* **2014**, *32*, 997−1006. in Chinese with English abstract.
(53) Condie, K. C. Chemical composition and evolution of the upper continental crust: Contrasting results from surface samples and shales. *Chem. Geol.* **1993**, 1−37.
(54) Chen, L.; Guo, F.; Steel, R. J.; Li, Y. Petrography and geochemistry of the Late Cretaceous redbeds in the Gan-Hang Belt, southeast China: implications for provenance, source weathering, and tectonic setting. *Int. Geol. Rev.* **2016**, *58*, 1196−1214.
(55) Chen, L. Q. *Late Cretaceous sedimentary evolution of Yongchong Basin, Jiangxi Province*; Beijing, Geological Publishing House 2018, 1 −118 in Chinese.
(56) Taylor, S. R.; McLennan, S. M. *The Continental Crust: Its Composition and Evolution*. Blackwell Scientific Publications: Oxford. 1985, pp. 1- 312.
(57) Johnsson, M. J. The system controlling the composition of clastic sediments. *Spec. Pap. - Geol. Soc. Am.* **1993**, *284*, 1−20.
(58) Yang, X.; Cheng, X.; Zhou, Y.; Ma, L.; Zhang, X.; Yan, Z.; Peng, X.; Su, H.; Wu, H. Paleomagnetic results from Late Carboniferous to Early Permian rocks in the northern Qiangtang terrane, Tibet, China, and their tectonic implications. *Sci. China Earth sci.* **2017**, *60*, 124−134.
(59) Nesbitt, H. W.; Young, G. M. Early Proterozoic climates and plate motions inferred from major element chemistry of lutites. *Nature* **1982**, *299*, 715−717.
(60) Fedo, C. M.; Nesbitt, H. W.; Young, G. M. Unraveling the effects of potassium metasomatism in sedimentary rocks and paleosols, with implications for paleoweathering conditions and provenance. *Geology* **1995**, *23*, 921−924.
(61) Rudnick, R. L.; Gao, S. Composition of the continental crust. *Treatise Geochem.* **2003**, *3*, 1−64.
(62) Nesbitt, H. W.; Young, G. M. Formation and diagenesis of weathering profiles. *J. Geol.* **1989**, *97*, 129−147.
(63) McLennan, S. M.; Hemming, S.; McDaniel, D. K. Geochemical Approaches to Sedimentation, Provenance and Tectonics. *Spec. Pap. - Geol. Soc. Am.* **1993**, 21−40.
(64) Xu, X. T.; Shao, L. Y. Limiting factors in utilization of chemical index of alteration of mudstones to quantify the degree of weathering in provenance. *J. Palaeogeogr.* **2018**, *20*, 515−522. in Chinese with English abstract.
(65) Nesbitt, H. W.; Young, G. M. Prediction of some weathering trends of plutonic and volcanic rocks based on thermodynamic and

kinetic considerations. *Geochim. Cosmochim. Acta* **1984**, *48*, 1523−1534.

(66) Potter, P. E. Petrology and chemistry of modern big river sands. *J. Geol.* **1978**, *86*, 423−449.

(67) Roser, B. P.; Cooper, R. A.; Nathan, S.; Tulloch, A. J. Reconnaissance sandstone geochemistry, provenance, and tectonic setting of the Lower Paleozoic terranes of the West Coast and Nelson, New Zealand. *N. Z. J. Geol. Geophys.* **1996**, *39*, 1−16.

(68) Roser, B. P.; Korsch, R. J. Provenance signatures of sandstone-mudstone suites determined using discriminant function analysis of major-element data. *Chem. Geol.* **1988**, *67*, 119−139.

(69) Bhatia, M. R.; Crook, K. A. W. Trace element characteristics of graywackes and tectonic setting discrimination of sedimentary basins. *Contrib. Mineral. Petrol.* **1986**, *92*, 181−193.

(70) Pettijohn, F. J.; Potter, P. E.; Siever, R. *Sand and Sandstone*; Springer-Verlag: New York, 1972, pp. 1-553.

(71) Shao, L.; Stattegger, K.; Garbe-Schoenberg, C. D. Sandstone petrology and geochemistry of the Turpan Basin (NW China): Implications for the tectonic evolution of a continental basin. *J. Sediment. Res.* **2001**, *71*, 37−49.

(72) Roser, B. P.; Korsch, R. J. Determination of tectonic setting of sandstone-mudstone suites using SiO2 content and K2O/Na2O ratio. *J. Geol.* **1986**, *94*, 635−650.

(73) Chen, H. H.; Wu, Y.; Xiao, Q.; He, G. S. Evidence of fluid inclusions from ancient reservoirs in Qamdo Basin. *Acta Geol. Sin.* **2010**, *84*, 1457−1469. in Chinese with English abstract.

(74) Du, H. F.; Jiang, Y. B.; Yan, Z. B.; Hou, Z. Q.; Yang, T. N.; Guo, F. S.; Yang, Q. K. Sedimentary Characteristics and Environment of the Paleogene Nangqian Basin in Qinghai Province. *Acta Geol. Sin.* **2011**, *85*, 383−395. in Chinese with English abstract.

(75) Du, H. F.; Jiang, Y. B.; Hou, Z. Q.; Yan, Z. B.; Guo, F. S.; Guo, G. L. Geochemical characteristics of Paleogene sandstones in Nangqen basin and their implications for provenance and sedimentary environments. *Acta Petrol. Mineral.* **2011**, *30*, 654−664. in Chinese with English abstract.

(76) Du, H. F.; Zhu, Z. J.; Jiang, Y. B.; Yang, T. N.; Liu, Y. X.; Guo, F. S. Petrological characteristics and provenance analysis of sandstones of Gonjo Formation in Nangqen basin. *Acta Petro. Mineral.* **2011c**, *30*, 401−408. in Chinese with English abstract.

(77) Jian, X.; Weislogel, A.; Pullen, A. Triassic Sedimentary Filling and Closure of the Eastern Paleo-Tethys Ocean: New Insights from Detrital Zircon Geochronology of Songpan-Ganzi, Yidun, and West Qinling Flysch in Eastern Tibet. *Tectonics* **2019**, *38*, 767−787.

(78) Cullers, R. The controls on the major and trace element variation of shales, siltstones and sandstones of Pennsylvanian-Permian age from uplifted continental blocks in Colorado to platform sediment in Kansas, USA. *Geochim. Cosmochim. Acta* **1994**, *58*, 4955−4972.

(79) Wei, W.; Algeo, T. J. Elemental proxies for paleosalinity analysis of ancient shales and mudrocks. *Geochim. Cosmochim. Acta* **2020**, *287*, 341−366.

(80) Zhou, Y.; Cheng, X.; Wu, Y.; Kravchinsky, V.; Shao, R.; Zhang, W.; Wei, B.; Zhang, R.; Lu, F.; Wu, H. The northern Qiangtang Block rapid drift during the Triassic Period: paleomagnetic evidence. *Geosci. Front.* **2019**, *10*, 2313−2327.

(81) Song, P.; Ding, L.; Lippert, P. C.; Li, Z.; Zhang, L.; Xie, J. Paleomagnetism of middle Triassic lavas from Northern Qiangtang (Tibet): constraints on the closure of the Paleo-Tethys ocean. *J. Geophys. Res.: Solid Earth* **2020**, *125*, No. e2019JB017804.

(82) Guan, C.; Yan, M.; Zhang, W.; Fu, Q.; Liang, Y.; Xu, W.; Zan, J.; Li, B.; Zhang, T.; Shen, M. Paleomagnetic and chronologic data bearing on the Permian/Triassic boundary position of Qamdo in the Eastern Qiantang Terrane: implications for the closure of the Paleo-Tethys. *Geophys. Res. Lett.* **2021**, *48*, No. e2020GL092059.

(83) Yu, L.; Yan, M.; Domeier, M.; Guan, C.; Chen, M.; Fu, Q.; Xu, W.; Xu, Z.; Niu, Z.; Yang, L.; Rwn, D.; Zhang, W.; Zan, J.; Zhang, D.; Li, B. New paleomagnetic and chronological constraints on the Late Triassic position of the Eastern Qiangtang Terrane: Implications for the closure of the Paleo-Jinshajiang Ocean. *Geophys. Res. Lett.* **2022**, *49*, No. e2021GL096902.

(84) Tian, J. C.; Zhang, X. *Sedimentary geochemistry*; Beijing, Geological Publishing House, 2016. (in Chinese).

(85) Zheng, Y.; Anderson, R. F.; van Geen, A.; Kuwabara, J. Authigenic molybdenum formation in marine sediments: a link to pore water sulfide in the Santa Barbara Basin. *Geochim. Cosmochim. Acta* **2000**, *64*, 4165−4178.

(86) Morford, J. L.; Martin, W. R.; Carney, C. M. Uranium diagenesis in sediments underlying bottom waters with high oxygen content. *Geochim. Cosmochim. Acta* **2009**, *73*, 2920−2937.

(87) Morford, J. L.; Martin, W. R.; Francois, R.; Carney, C. M. A model for uranium, rhenium, and molybdenum diagenesis in marine sediments based on results from coastal locations. *Geochim. Cosmochim. Acta* **2009**, *73*, 2938−2960.

(88) Helz, G. R.; Miller, C. V.; Charnock, J. M.; Mosselmans, J. F. W.; Pattrick, R. A. D.; Garner, C. D.; Vaughan, D. J. Mechanism of molybdenum removal from the sea and its concentration in black shales: EXAFS evidences. *Geochim. Cosmochim. Acta* **1996**, *60*, 3631−3642.

(89) Tribovillard, N.; Riboulleau, A.; Lyons, T.; Baudin, F. Enhanced trapping of molybdenum by sulfurized organic matter of marine origin as recorded by various Mesozoic formations. *Chem. Geol.* **2004**, *213*, 385−401.

(90) Wei, H.; Wei, X.; Qiu, Z.; Song, H.; Shi, G. Redox conditions across the G-L boundary in South China: Evidence from pyrite morphology and sulfur isotopic compositions. *Chem. Geol.* **2016**, *440*, 1−14.

(91) Wei, H.; Shen, J.; Schoepfer, S. D.; Krystyn, L.; Richoz, S.; Algeo, T. J. Environmental controls on marine ecosystem recovery following mass extinctions, with an example from the Early Triassic. *Earth-Sci. Rev.* **2015**, *149*, 108−135.

(92) Wei, H.; Algeo, T. J.; Yu, H.; Wang, J.; Guo, C.; Shi, G. Episodic euxinia in the Changhsingian (late Permian) of South China: Evidence from framboidal pyrite and geochemical data. *Sediment. Geol.* **2015**, *319*, 78−97.

(93) Calvert, S. E.; Pedersen, T. F. Geochemistry of recent oxic and anoxic marine sediments: implications for the geological record. *Mar. Geol.* **1993**, *113*, 67−88.

(94) Klinkhammer, G. P.; Palmer, M. R. Uranium in the oceans: where it goes and why. *Geochim. Cosmochim. Acta* **1991**, *55*, 1799−1806.

(95) Wei, H.; Tang, W.; Gu, H.; Fu, X.; Zhang, X. Chemostratigraphy and pyrite morphology across the Wuchiapingian-Changhsingian boundary in the Middle Yangtze Platform, South China. *Geol. J.* **2021**, *56*, 6102−6116.

(96) Wei, H.; Zhang, X.; Qiu, Z. Millennial-scale ocean redox and δ13C changes across the Permian-Triassic transition at Meishan and implications for the biocrisis. *Int. J. Earth Sci.* **2020**, *109*, 1753−1766.

(97) Wei, H.; Tang, Z.; Qiu, Z.; Yan, D.; Bai, M. Formation of large carbonate concretions in black cherts in the Gufeng Formation (Guadalupian) at Enshi, South China. *Geobiology* **2020**, *18*, 14−30.

(98) Wei, H.; Chen, D.; Wang, J.; Yu, H.; Tucker, M. E. Organic accumulation in the lower Chihsia Formation (Middle Permian) of South China: Constraints from pyrite morphology and multiple geochemical proxies. *Palaeogeogr. Palaeoclimatol. Palaeoecol.* **2012**, *353-355*, 73−86.

(99) Wei, H.; Chen, D.; Yu, H.; Wang, J. End-Guadalupian mass extinction and negative carbon isotope excursion at Xiaojiaba, Guangyuan, Sichuan. *Sci. China Earth Sci.* **2012**, *55*, 1480−1488.

(100) Tribovillard, N.; Algeo, T. J.; Lyons, T.; Riboulleau, A. Trace metals as paleoredox and paleoproductivity proxies: an update. *Chem. Geol.* **2006**, *232*, 12−32.

(101) Algeo, T. J.; Li, C. Redox classification and calibration of redox thresholds in sedimentary systems. *Geochim. Cosmochim. Acta* **2020**, *287*, 8−26.

(102) Algeo, T. J.; Tribovillard, N. Environmental analysis of paleoceanographic systems based on molybdenum-uranium covariation. *Chem. Geol.* **2009**, *268*, 211−225.

(103) McLennan, S. M. Relationships between the trace element composition of sedimentary rocks and upper continental crust. *Geochem., Geophys., Geosyst.* **2001**, *2*, No. 1021.

https://doi.org/10.1021/acsomega.3c03144
ACS Omega 2023, 8, 26458−26478

(104) Scott, C.; Lyons, T. W. Contrasting molybdenum cycling and isotopic properties in euxinic versus non-euxinic sediments and sedimentary rocks: Refining the paleoproxies. *Chem. Geol.* **2012**, *324-325*, 19−27.
(105) Zhu, R.; Zhao, P.; Zhao, L. Tectonic evolution and geodynamics of the Neo-Tethys Ocean. *Sci. China Earth Sci.* **2022**, *65*, 1−24. in Chinese with English abstract.
(106) Peng, Y.; Liu, H.; Feng, Z. Analysis and correlation of Triassic sequence stratigraphy in eastern Tibet. *Zhongguo Kuangye Daxue Xuebao (J. China Univ. Min. Technol.)* **2000**, *06*, 51−55. in Chinese with English abstract.
(107) Bian, Z. X. *Provenance analyses on Paleogene clastic rock in Gonjo basin:implications for tectonic evolution*; Kunming,Yunnan University, 2021. in Chinese with thesis.
(108) Nie, Y.; Fu, X.; Wei, H.; Lin, F.; Zeng, S.; Mansour, A.; Zhou, G.; Wang, W. Paleoenvironmental reconstruction preceding and during the early Aptian Oceanic Anoxic Event 1a in southern Tibet, eastern Tethys. *Cretaceous Res.* **2023**, *150*, No. 105604.
(109) Nie, Y.; Fu, X.; Liu, X.; Wei, H.; Zeng, S.; Lin, F.; Wan, Y.; Song, C. Organic matter accumulation mechanism under global/regional warming: Insight from the Late Barremian calcareous shales in the Qiangtang Basin (Tibet). *J. Asian Earth Sci.* **2023**, *241*, No. 105456.

https://doi.org/10.1021/acsomega.3c03144
ACS Omega 2023, 8, 26458−26478